Screening and simulation of offshore CO2-EOR and storage

Screening and simulation of offshore CO_2-EOR and storage: A case study for the HZ21-1 oilfield in the Pearl River Mouth Basin, Northern South China Sea

Pengchun Li[a,b,c] Linzi Yi[d] Xueyan Liu[a] Gang Hu[c] Jiemin Lu[e] Di Zhou[a,f] Susan Hovorka[e] Xi Liang[f,g]

a CAS Key Laboratory of Ocean and Marginal Sea Geology, South China Sea Institute of Oceanology, Chinese Academy of Sciences, Guangzhou, China

b State Key Laboratory of Oil and Gas Reservoir Geology and Exploitation (Chengdu University of Technology), Chengdu, China

c Guangdong Research Center for Unconventional Energy Engineering Technology, Guangdong University of Petrochemical Technology, Maoming, China

d Key Laboratory of Renewable Energy, Guangzhou Institute of Energy Conversion, Chinese Academy of Sciences, Guangzhou, China

e Gulf Coast Carbon Center, Bureau of Economic Geology, The University of Texas at Austin, TX, United States

f UK-China (Guangdong) CCUS Centre, Guangzhou, China

g Business School, University of Edinburgh, United Kingdom

Abstract: CO_2-enhanced oil recovery (CO_2-EOR) and storage is currently the most effective and economic technology for reducing CO_2 emissions from burning fossil fuels in large scale. This paper is the first effort of proposing a modelling assessment of CO_2-EOR and storage in the HZ2-1 oilfield in the Pearl River Mouth Basin in northern South China Sea offshore Guangdong Province. We attempt to couple the multi-parameter dimensionless quick screening model and reservoir compositional simulation for optimization of site screen and injection simulation. Through the quick screening, the reservoirs are ranked by EOR dimensionless recovery R_D, and by CO_2 storage in pore volume S_{CO2}. Our results indicate that S_{CO2} is highly pressure dependent and not directly related to R_D. Of these reservoirs, CO_2-EOR and storage potential of the M10 was estimated through a compositional simulation as a case study based on a 3D geological model. Nine scenarios of CO_2 injection operations have been simulated for 20 years with different well patterns and injection pressures. The simulation results represent an obvious improvement in oil production by CO_2 flooding over No-CO_2 production. The best operation for M10 is miscible CO_2 flooding, which led to the higher recovery factors of 52%~58% and CO_2 stored masses of 8.1×10^6~10.8×10^6t. The optimum operation for CO_2 injection should be set well pattern in region of injector I1 and high injection pressure for miscible flooding. In a whole, the HZ21-1 field can be used as a candidate geological site for GDCCUS project. We are fully aware of the limitation in the primary modelling including reservoir and fluid properties and production history matching, and regard this study as a general and hypothetic proposal.

Keywords: CO_2-EOR; CO_2 storage; Quick screening; Compositional simulation; Offshore HZ21-1oilfield

1. Introduction

Carbon capture and storage (CCS) is regard as the key strategy for large scale decarbonisation from burning fossil fuels (Aminu et al., 2017; Liu et al., 2017). In addition, carbon capture, utilization and storage (CCUS) emphasizes

the utilization of the captured CO_2 together with storage, CO_2 Enhanced Oil Recovery (CO_2-EOR) is the major form of CCUS (Li et al., 2016; Liu et al., 2017). Many countries have participated in activities to address global climate changes over the last few years. Based on the statistics of Global Status 2018, 39 large-scale CCUS projects were in operation or under construction and planning. Of the 15 projects are in operation, 12 are related to CO_2 Enhanced Oil Recovery (CO_2-EOR) (GCCSI, 2016). CO_2-EOR has been widely studied and successfully applied in the United States and is a relatively mature technology in theory and application (Azzolina et al., 2015; Kuuskraa and Wallace, 2014; Qin et al., 2015; Shen et al., 2007; Shen and Liao, 2009). China is one of the most active countries in CCUS activities (Li et al., 2016; Liu et al., 2017). There are currently 12 large scale integrated projects (LSIPs) at various stages throughout China (Li et al., 2016). Interest in CO_2-EOR as the most effective technique of CCUS has been increasing in China since the beginning of this century. A number of CO_2-EOR field tests have been carried out in Jilin, Dagang, Shengli, Zhongyuan, Yanchang and Liaohe oilfields, with recovery factor increasing to approximately 10% (Liu et al., 2017). However, these projects have focused on onshore oilfields, none on offshore so far (Bi et al., 2011; Hao and Song, 2010; Jiao et al., 2014; Liu and Gao, 1995; Luo et al., 2013; Zhao et al., 2014; Zhu and Chen, 2007).

There have been few offshore CO_2-EOR projects around the world, but this has changed in recent decades due to the advances of CCUS under the high demand for carbon reduction (DiPietro et al., 2015; Kuuskraa and Malone, 2016; Malone et al., 2014). By the end of 2017, several significant offshore CO_2-EOR efforts were underway. UK and USA have completed CO_2-EOR feasibility assessments for the UK North Sea continental shelf and the Gulf of Mexico, respectively. Several CO_2-EOR pilot tests have been conducted offshore Arabian Sea, Vietnam, and Malaysia Sarawak. "Next generation" CO_2-EOR techniques have been applied on a commercial scale in the deep water Lula oil field offshore Brazil (Malone et al., 2014). Successful CO_2-EOR applications offshore fields has been steadily increasing, which indicates that CO_2-EOR applications in offshore oilfields are receiving significant attention (Kang et al., 2016).

Guangdong Province has the largest economic aggregate in China with large CO_2 emissions (Huang et al., 2013). Most large CO_2 point sources (thermal power plants, iron, steel and petrochemical plants) in Guangdong are distributed along the southeast coast (Huang et al., 2013; Zhou et al., 2013a) (Fig. 1). Guangdong has small onshore sedimentary basins and is densely populated, so it provides limited and unfavourable conditions for large scale CO_2 geological storage. In contrast, large sedimentary basins are present offshore. In particular, the Pearl River Mouth Basin (PRMB) contains thick sedimentary layers with high porosity and permeability reservoirs, which could provide sufficient capacity for storing the CO_2 emitted from the large point sources along the coast (Li et al., 2013; Zhou et al., 2011). The necessity and feasibility of CCUS in Guangdong have been confirmed by a study in 2010-2013 (Zhou et al., 2013b). Offshore storage is recognized as the preferred option of CO_2 storage for Guangdong (Li et al., 2013; Zhou et al., 2013b), which led to the promotion of the Guangdong offshore CCUS project (GOCCUS) (Zhou et al., 2018). The GOCCUS team is prepared for the long-term and large-scale development of offshore CO_2 utilization and storage for Guangdong in 2030 and 2050 (Zhou et al., 2018). Efforts in CO_2 utilization and storage have concentrated on identifying early opportunities (Li et al., 2018; Li et al., 2015), which are believed to be in the producing oilfields in

the PRMB. Three of oilfields (HZ21-1, HZ32-3 and XJ24-3) were selected as candidates for the first CCUS demonstration project, and HZ21-1 is currently considered the most favourable (Li et al., 2015; Zhou et al., 2018). The assessment of CO_2-EOR and storage potential in HZ21-1 becomes essential. Therefore, in this paper, a workflow that couples a multi-parameter quick screening model and multiphase flow program is applied to quantitatively analyse the optimum site and capacity for CO_2-EOR and storage in the HZ21-1 field. We performed quick screening of the 6 main oil reservoirs in the field and recognized M10 as the most promising reservoir. A 3D geological model for M10 was built as a case study, and compositional simulations for 9 injection scenarios and a No-CO_2 scenario were performed to evaluate the potential of CO_2-EOR and storage. This is the first attempt to evaluate the potential of both CO_2-EOR and storage potential in the PRMB at the reservoir scale. We hope that the results could provide a start and reference for further development of offshore CO_2-EOR and storage in the PRMB, as well as in the basins offshore southeast China.

2. Background

2.1 Geography and geology

The Pearl River Mouth Basin (PRMB), 111°20′~118°0′E and 18°30′~23°00′N, is the largest sedimentary basin in the northern South China Sea offshore Guangdong Province. The HZ21-1 field, located ~160 km southeast of Hong Kong and ~170 km from Daya Bay, is the earliest producing field in the PRMB (Fig. 1). Geologically, the HZ21-1 field is a 10.5 km^2 gentle dome draped over a basement high (Fig. 2). Reservoir rocks are uppermost Oligocene Zhuhai formation (Fm.) to Lower Miocene Zhujiang Fm. sandstones of littoral to delta-front/neritic facies. Thick mudstone cap rocks at 2676~2850 m directly overlying oil reservoirs are of breakthrough pressure up to 20 MPa (Chen et al., 2007). A EW-trending fault is located in the north, which is 1.6 km long and has >30 m of throw (Fig. 2). The fault cuts through mudstone layers, filled with argillaceous gouge, and is considered to be a sealing fault (Liu, 2011; Zhai and Wang, 1990; Zhu et al., 2010).

HZ21-1 is only field in the PRMB that contains both oil and gas reservoirs. There are two gas condensate reservoirs in the upper part (2420-2580 m) and eight oil reservoirs in the lower part (2850-3060 m) (Fig. 3). The thicknesses of reservoirs range from 1.9 to 43.4 m, the structurally closed areas from 7.2 to 9.7 km^2, and the closure heights from 11.5 to 23.0 m (Liu, 2011; Zhu et al., 2010). Core data indicate that these reservoirs have porosity of 12.8-16.6% and permeability of 68-317.3 mD. The reservoirs in HZ21-1 have mostly edge water, except L60, M10, and M12 with bottom water. The water energy is strong, and water flood is proved unnecessary (Liu, 2011). The HZ21-1 field produces light crude oil with formation density of 0.641-0.727 g/cm^3 and viscosity of 0.33-0.74 mPa·s, and surface density of 0.797-0.812 g/cm^3, API gravity of 42.8-46, and viscosity of 1.2-2.8 mPa·s. The proven geological reserves of crude oil are $1,575.00\times10^4$ t, the technically recoverable reserves are 752×10^4 t, and the economically recoverable reserves are 729.6×10^4 t (Liu, 2011).

2.2 Reservoir characteristics

The general parameters for the oil reservoirs in HZ21-1, as listed in Table 1, vary little horizontally. The three oil reservoirs (L30, L60, and M10) have similar production responses within the entire region, and the M10 oil reservoir extends >200 km in the E-W direction. Of the 8 oil reservoirs, the L45 and M12 reservoirs are not considered in this study because they are very thin and have limited proven reserves less than 50,000 m^3. Other 6 reservoirs are studied to evaluate the CO_2-EOR and storage potential.

M10 is the largest reservoir in the field, with geological reserves of 6.37 $\times 10^6$ m^3, accounting for 33% of the total field reserves (Liu, 2011). This reservoir resides at depths near 3000m (Fig. 2), consists of cross-bedded glutenite and upward-fining sandstone of beach facies. Sandstone represents 91% of the total thickness and is relatively constant (Fig. 3). Core test data show that the average permeability of M10 reservoir is 205.3 mD, and the average porosity is 15.3%. The original reservoir pressure is 4325 psi, and the temperature is 132 ºC. The rock is hydrophilic, and the oil-water contact is at a depth of ~2,961 m with an oil column height of 22.5 m. The crude oil has a reservoir density and viscosity of 0.747 g/cm^3 and 0.32 mPa·s, respectively. The natural bottom water drive energy of M10 is very strong, thus, the water flooding was unnecessary. In terms of offshore CO_2-EOR screening criteria (Kang et al., 2016), the high-quality light oil and the significant depths (approximately 3000 m) of the reservoirs suggest the possibility of miscible CO_2 flooding, but the small amount of original oil in place and the high proportion of primary oil recovery (which suggests a low residual oil saturation) might limit the potential for CO_2 flooding.

2.3 Production history

The HZ21-1 field began oil production in 1990 and gas production in 2005. The oil was produced at high rates (>5.5%) for the first 4 years and was then stabilized through re-perforating, lateral wells and other measures. The oil recovery factor reached 19.34% in 1993, 23.18% in 1997 and 29.7% in 2005 with a cumulative oil production of 1,189.87×10^4 stb (Liu, 2011).

3. Data and methodology

3.1 Data set and property parameters

The data used in this study are all from a database compiled by SCSIO (South China Sea Institute of Oceanology, Chinese Academy of Sciences) by collecting industry data in published papers, books, reports and atlases.

3.1.1 Reservoir property parameter set

Table 2 shows a list of the reservoir property parameters including rock and fluid properties and engineering information which refer from Li et al. (2018) and Liu (2011). In this paper, the reservoir dip (α) was set as a constant value of 3.5° according to actual formation dip in these reservoirs as described in Liu (2011). Because water flooding was not conducted in HZ21-1 field and we only have the data of total recovery factors. The initial oil saturation (S_{oi}), which represents the oil saturation at the beginning of CO_2 injection, is calculated based on Li et al. (2018).

3.1.2 Well log interpretations

Gamma ray (GR) logs of six wells are shown in the left columns in Fig. 4 for M10 reservoir. Following the previous study of micro-facies of the Zhujiang Formation (Chen et al., 2012; Lei et al., 2015; Li et al., 2008; Shi et al., 1999), the depositional lithofacies of the model were built in the Petrel platform according to a reinterpretation of the sequence stratigraphic framework based on GR logs and a new depositional model of shallow marine sandstone. This was used to control the horizontal distributions of the porosity and permeability. As shown in column 2 of Fig.4, the identified lithofacies are mainly transitional bar (50.93% of the total volume), secondary inner bar (18.6%), outer bar (12.4%), beach-A (13.4%), small volumes of beach-B (3.7%) and muddy sand (1.0%). The porosity and permeability were then interpreted from the well logs in Petrel system. According to the #1 well log and core test data (GR, porosity Φ and permeability k), following Timur (1968), we matched the relationships between these parameters as:

$$\Phi = \ln (0.2394 / V_{sh}) / 5.121 \quad (1)$$

$$K = 2.028 \times \Phi^{6.7859} / S_{wir}^{2} \quad (2)$$

where Φ is the porosity, %; V_{sh} is the mud content, f; K is the permeability, mD; S_{wir} is the residual water saturation, %. Formula 2 was rewritten by regression calculation from Timur's equation $K = (0.136 \times \Phi^{4.4})/S_{wir}^{2}$ to $K = (C \times \Phi^{x})/S_{wir}^{y}$ according to Du and Zhang (2000), where C is the discriminant coefficient for lithofacies. Φ was set as value of 15.3%, and S_{wir} as 26% during regression calculating. V_{sh} is calculated as follows:

$$V_{sh} = (2^{GCUR \times Ish} - 1) / (2^{GCUR} - 1) \quad (3)$$

$$I_{sh} = (GR - GR_{min}) / (GR_{max} - GR_{min}) \quad (4)$$

where GCUR is the hilchie index, which is given as 3.7 because the M10 is Neogene in age (Fertl and Frost, 1980); I_{sh} is gamma ray shale index, f; GR is the value of gamma ray log, API; GR_{min} is the gamma ray value of sandstone, API; GR_{max} is the gamma ray value of mudstone, API. Using Formulas 1 and 2, porosity and permeability of 5 well groups have been calculated, of which are shown in columns 3 and 4 of Fig. 4, respectively, to control their vertical variations in the property model.

3.1.3 Equation of state (EOS)

As detailed oil composition data were not available, the composition of the crude oil were simulated using WINPROP's 'Recombination' option based on the industry test and experimental data including oil chromatogram, gas/oil ratio, dissolved gas content, oil density, and viscosity (Liu, 2011; Wang et al., 1990). This resulted in an 8-component crude oil system with 6 light components (CO_2, CH_4, C_2H_6, C_3H_8, C_4H_{10} and C_5H_{12}) and 2 heavy components (C_6^+, which represents C_6-C_{12}, and C_{13}^+, which represents C_{13}-C_{35}). We then matched them in WINPROP with the experimental data of oil properties available from PVT and viscosity tests through the regression parameters Omega A and Omega B. The resulted oil composition was listed in Table 3, which has a formation viscosity of 0.32 mPa·s and formation density of 0.706 g/cm^3.These are all very similar to the properties of experimental data, implying

a good match. Finally, the equation of state (EOS) for the 8-component oil was established based on the Peng-Robinson formulation. The output file including fitted EOS and the parameters were exported into GEM compositional model to simulate fluid behaviour at different conditions.

3.1.4 Determination of CO_2 minimum miscible pressure

To determine the minimum miscible pressure *(MMP)* for the CO_2 flooding in the M10 reservoir, a set of 1D compositional models mimicking slim tubes were used at a range of reservoir temperatures and pressures. In our simulation, the slim-tube model has 500 grid cells; each is 9 cm long, 11 cm wide and 11 cm high. The temperature, porosity and permeability were set to the reservoir conditions of 132°C, 0.15 and 205 mD, respectively. The initial formation pressure varies from 2000 psi to 5500 psi. The injector is on the left side of the slim tube, and the producer is on the right side. The injection pressure and production pressure vary with the initial pressure, and the difference between them is kept constant at 200 psi. The results show that when the injection pressure reached ~4400 psi (Fig. 5), the oil recovery factor stopped increasing rapidly. This indicates that *MMP* is ~4400 psi, which is slightly higher than the original formation pressure (~4300 psi) in the M10 reservoir.

3.2 Reservoir screening

The objective of a CO_2-EOR potential evaluation in a carbon-sequestration environment is to estimate the oil-recovery efficiency and the volume of sequestered CO_2 in various operating scenarios (Shaw and Bachu, 2002). Although a reservoir simulation can be used for a relatively precise capacity assessment if detailed reservoirs data are available, the potential of CO_2-EOR and storage must first be evaluated quantitatively to determine the oil recovery and CO_2 storage capacities. Thus, the quick prediction of CO_2 flooding performance is expressed in relation to the target original oil in place (OOIP) (Hendriks et al., 2004; Shaw and Bachu, 2002). A dimensionless model, developed by Wood (2006), is invoked to quickly screening 6 oil reservoirs in HZ21-1 oilfield (excluded M12 and L45 reservoir due to the little reserve under 50,000 m^3), so as to primarily quantify oil recovery potential as well as CO_2 storage capacity by ranking, which can qualify the most representative and promising reservoir for compositional modelling. Established on basis of Gulf of Mexico Coast reservoirs, this model is more adaptable than other screening models (e.g. Rivas et al, 1992) in aspects of small databases of different reservoirs and taking CO_2 storage into consideration. On top of that, high permeability (>100 mD) in offshore reservoirs are similar in both Gulf Coast and Guangdong Coast areas.

Five dimensionless output groups developed in this model presents oil breakthrough time ($t_D{}^o$), recovery factor at CO_2 injection of 0.8 PV (R_{D1}), 1.0 PV (R_{D2}) and 1.2 PV (R_{D3}) and CO_2 storage capacity (S_{CO2}). Seven dimensionless input groups for calculating these 4 screening parameter groups involve in R_L (Effective aspect ratio), M_g (Mobility ratio), N_g (Buoyancy number), P_{injD} (Injection pressure group), P_{pD} (Production pressure group), S_{oi} (Initial oil saturation) and S_{orw} (Residual oil saturation) with formulas listed in Table 4. Especially, S_{oi} stands for initial oil saturation at the beginning of CO_2 flooding.

3.3 Reservoir numerical modelling

3.3.1 Model configuration

A structural model for the M10 reservoir as shown in Fig. 6 was built in Petrel platform based on the following data: reservoir surface contour map (Fig. 2), nearly NS formation cross section (Fig. 3), GR logs from 6 wells and complete log data from the #1 well and interpretation (Fig. 4). The model is 4200 m long and 3800 m wide, has an average thickness of 41.7 m, and covers the entire area except for aquifers at depths from 2934.5 m to 3058.7 m. The model consists of 86×76×23 (total of 146,832) corner-point cells, and each cell is approximately 50×50×1.72 m. To provide sufficient bottom water energy and match the oil production history, the southern and eastern boundaries were set to be closed, and the western boundary was set to be open, where infinite bottom water enters to mimic the strong bottom water energy. Interpolation with a Gaussian Random Simulation process was used to construct a 3D porosity model and permeability model (Fig. 7). The average porosity and permeability in the 3D property model are 15.84% and 212.35 mD, respectively. The error is <4% compared with the real field core data (porosity 15.3% and permeability 205.3 mD, respectively), which indicates that the 3D property model is reliable and can be used in further simulations.

3.3.2 Relative permeability

The water-oil relative permeability (*Kr*) curves were measured from a total 18 steady-state core samples of M10 reservoir. The normalized relative permeability curves of the oil-water phases are shown in Fig. 8(a). The gas-oil imbibition relative permeability curves ware calculated by pore scale model based on the experimental data of relative permeability in displacement process of Fig. 8a (Liu, 2011). The air-*NaCl* capillary pressure (*Pc*) curve was measured from 29 core samples using semipermeable-membrane method. Initial water saturations were established using $J(S_w)$ Function approach as a function of height above the oil water contact and rock quality (porosity and permeability). The normalized capillary pressure curve was shown in Fig.8b (Liu, 2011). These curves were input into the model and used throughout the entire model process and the curve shapes will be modified to match the history.

3.3.3 Initialization and history match

Based on the reservoir model described above, well positions were chosen to be representative of the actual positions of the wells. The model was initialized as conditions at the beginning of production from the field. The history matching was then performed to match the pre-CO_2 flooding production history of the M10 reservoir using the GEM simulator. Modifications were made to the reservoir properties, including the relative permeability and capillary pressure, and well productivity indices, to match the oil reserves and oil and water production rates of the reservoir. After several simulation runs, we obtained a good history match with the production history data including cumulative oil production, recovery factor and water cut. The results show that the oil recovery factor in 2005 was 29.2% and the cumulative oil production was 1178.44×10^4 stb, which are very close to the production history data. The reserve of the M10 model is 4030.92×10^4 stb, which is approximately equal to the oilfield reserves of 4006.29×10^4 stb. After the history matching, the reservoir mode is assumed to be an approximation of the field in terms of the pressure and

residual oil saturation. The simulation then continued from 2005 to 2016 to predict the pressure and oil distribution at the start of the CO_2 injection. The results of the simulation are shown in Fig. 9a, where the initial oil saturation in 1990 is 0.5-0.6 and is higher in the northern reservoir. However, after 26 years of primary production, the residual oil saturation is 0.29-0.59 as shown in Fig. 9b and is higher in the south, which might be because the production wells are more concentrated in the northern region.

3.3.4 Simulation scenario design

After the history matching process, the model is used to simulate and predict different CO_2 injection scenarios. The locations and settings of the oil production wells are the same as those used in the primary production. Two existing wells (#9A and #3), which are not producing, were set as CO_2 injectors with new names: injection wells 1 (I1) and 2 (I2) (see Fig. 9b for locations). These two wells are 800 m and 750 m from the closest production wells (#7 and #8, respectively). The injection pressures for the CO_2 injection wells were set to 5,000 psi, 5,500 psi and 6,000 psi. With a constant ratio of k_z/k_x(=0.1) and a constant injection pressure, 9 scenarios (A1, A2, A3, B1, B2, B3, C1, C2, C3) were set with various combinations of injection well(s) and well bottom pressures as listed in Table 5. Scenarios A, B and C represent scenarios using injection wells I1, I2, or I1 and I2, respectively, whereas the numbers 1, 2 and 3 represent injection pressures of 5,000 psi, 5,500 psi and 6,000 psi, respectively. The No-CO_2 (natural depletion production) scenario was also simulated and predicted. The time period of the simulation in all of the scenarios was 20 years (2016-2036).

4. Results and discussion

4.1 Quick screening results

By inputting reservoir property parameters of 6 reservoirs listed in Table 2 into an Excel spreadsheet calculator integrating formulas of screening model listed in Table 4, the five dimensional groups for site screening were calculated. The five outputs for quick screening of the 6 oil reservoirs are shown in Table 6 and its contrast trend lines also shown in Fig. 10 for comparison. The first critical output is the dimensionless oil breakthrough time (t_D^0), at which a significant amount of oil is recovered. For the model equation described as shown in Table 4, the most important fluid property groups in modelling t_D^0 were S_{oi} and S_{orw}, which are important in determining whether or not mobile oil is present at the beginning of CO_2 the flood. If mobile oil is present, oil will be produced almost immediately and therefore the t_D^0 will be close to zero, however, if only residual oil is present, oil will be produced much later in the flood and t_D^0 will be higher. The value of t_D^0 changes within the range of $0.61PV$ to $0.74PV$. The L30 and L50 have a t_D^0 larger than $0.7PV$, the L60, L40low and M10 have a very similar t_D^0 of $0.64PV$~$0.65PV$, and the L40up has a smallest t_D^0 of $0.61PV$. The residual oil will be recovered in larger quantities should lead a lower t_D^0 for miscible flooding. Therefore, the priority reservoir should be L30, L50, M10 and L40.

The changes of recovery were relatively large, with the changes of R_{D1} ranging from 4.2% to 36.13%, R_{D2} ranging from 8.89% to 51.27%, and R_{D3} ranging from 11.28% to 54.89%. The reservoir L60 has the highest R_D, followed by

M10, L40up and L50. This indicate that from the perspective of dimensionless recovery potential, the priority reservoir for EOR should be L60, M10, L40up and L50. Dimensionless CO_2 storage (S_{CO2}) is the only parameter indicating CO_2 storage potential. The S_{CO2} is relatively high, ranging from 0.78 to 0.81 *PV*. The maximum S_{CO2} is of L50 and L60, followed by M10 and L30, while L40up is the lowest. For the perspective of CO_2 sequestration, the higher is the S_{CO2}, the more is the potential of CO_2 stored. Therefore, the priority reservoir should be L50, L60, M10 and L30 with S_{CO2} greater than 0.8 *PV*.

As can be seen from the comparison curves in Fig. 10, the breakthrough time (t_D^0) and CO_2 storage (S_{CO2}) are basically horizontal, with little change, while the R_D varies relatively large, and there is no obvious similar correlation with the oil reserve (Q). Therefore, the screening of EOR and storage potential should mainly depend on R_D. The L60 and M10 reservoirs have the highest EOR recovery potential, with a final recovery factor (R_{D3}) of 54.89% and 52.49% of the initial residual oil, respectively. The L40up is the secondary reservoir, where 45.99% of the initial residual oil could be recovered by CO_2 flooding. Therefore, L60 and M10 are the most promising candidate reservoirs, followed by L40up, L50, L30 and L40low. Considering that the oil reserves of these three reservoirs, L60, M10 and L40up, are 70% of the total oil reservoirs over the entire field, CO_2-injection should be implemented in all these three reservoirs to obtain the best flooding effect. Because the reserves in the M10 reservoir are 33% of the total reserves and 2.7 and 1.7 times that in L60 and L40up, respectively, M10 has been produced more crude oil among the six reservoirs and has more industry and reservoir data, which are beneficial for further modelling evaluation as a case reservoir simulation study in this paper.

4.2 Reservoir simulation results

The simulation was run for all the 9 injection scenarios specified in 3.3.4, as well as for the No-CO_2 scenario. Resulted average reservoir pressure, ultimate oil recovery factor, and quantity of CO_2 storage are presented in Table 7. Although the estimated *MMP* is slightly higher than the original formation pressure in the M10 reservoir (see 3.1.4), these CO_2 injection scenarios have different flooding mechanisms. Scenarios A1, B1 and B2 are immiscible, A2, B3 and C1 are near-miscible, and A3, C2 and C3 are miscible flooding. This is because the reservoir pressure building up varies among the scenarios during the CO_2 flooding.

4.2.1 No-CO_2 production

The selected sector model includes 11 production wells (one horizontal well and ten vertical wells), and the bottom-hole pressure for the No-CO_2 scenario was set to 2,000 psi. The results are shown in Fig. 11. The oil production is in steady decline, and the reservoir is close to the end of its life. Fig. 11a shows the total oil production rate and water cut for the reservoir. The oil production rate decreases for more than 20 years of production, and the water cut increases to 98.4%. The total pressure drop is only 64 psi because of the strong reservoir bottom water energy. At the end of 20 years, the ultimate recovery factor only increases from 33.3% in 2016 to 37.4% in 2036 (Fig. 11b).

In fact, the primary oil production recovery factor of HZ2-1 is >45% (Liu, 2011). Obviously, the primary oil recovery

factor (37.4%) in this scenario is really lower than that of the actual recovery factor in production operator. The reason is that during the real 27 years' production history many enhanced measurements and well stimulations have been applied, which is very complicated and difficult to simulate. In our history matching process, those were ignored, leading to a lower ultimate primary recovery. But this recovery is only as a baseline of primary production for CO_2 flooding and does not affect the simulation and evaluation of CO_2 flooding.

4.2.2 Immiscible CO_2 flooding

The simulation models in scenarios A1, B1 and B2 were run with one CO_2 injection well and 11 production wells. The reservoir pressures are more stable and lower than *MMP* in scenarios A1 and B1, which suggest immiscible flooding. The reservoir pressure of scenario B2 varied significantly (Fig. 12a), slightly higher than *MMP* in the first 4 years, suggesting a short-lived miscible flooding. Then the reservoir pressure decreased to bellow *MMP* in the following 26 years suggesting immiscible flooding. So the CO_2-EOR in A1, B1 and B2 are considered as immiscible flooding in general.

The oil production rates of scenarios B1 and B2 increase rapidly in the early 4 years to a maximum rate of 2,192 bbl/day but subsequently decline (Fig. 12b). In contrast, although the production rate of A1 is not high initially, its decline is slower and with higher rate in late stage. The water cut declined differently among the scenarios (Fig. 12c). The decline of A1 is small in early stage, but it continues to decline in the middle stage, the water cut rose slowly and remained low value relatively in the later stage. The decline degrees of B1 and B2 are large in first 5 years, especially for B2 with lowest water cut in 2020, which affected by short-lived miscible flooding, but then go up very quickly and with high values in later stage. The recovery factors of B1 and B2 are high in early stage and with similar upward trend, but the recovery factor of A1 is goes up quickly in middle and later periods (Fig. 12d). The cumulative CO_2 stored in scenario A1 is 2.7 $\times 10^6$ t, which is more than in scenarios B1 and B2. The water cut is the lowest and the CO_2 stored potential is largest in A1, and the ultimate recovery factor at the end of 20 years is 45.08%, which is more than the No-CO_2 scenario, and the average reservoir pressure is 4,229 psi, which also higher than the No-CO_2 scenario. The scenario A1, therefore, should be the best immiscible scenario for CO_2 flooding and CO_2 storage.

4.2.3 Near-miscible CO_2 flooding

The simulation models in scenarios A2 and B3 were run with one CO_2 injection well with bottom pressures of 5,500 and 6,000 psi, and two CO_2 wells with bottom pressure of 5,000 psi in scenario C1. The production wells remained the same. As shown in Fig. 13a, the reservoir pressures of B3 and C1 are high than *MMP* in initial injection stage and then declined with different rate to bellow *MMP*. The reservoir pressure of B3 increases rapidly in the first 5 years to a maximum pressure of 4,839 psi and then decreases rapidly to below 4,400 psi, whereas the pressures in C1 are relatively stable, and its maximum pressures are lower than that in B3. As the average pressures of whole reservoir in scenarios A2, B3 and C1 (4395psi, 4325psi and 4331psi, respectively, Table 7) during CO_2 flooding are very close to the *MMP*, these scenarios are considered to be near-miscible

flooding in this paper.

The oil production rate of B3 increases rapidly in initial stage and up to a maximum rate of 2,700 bbl/day and maintain a high rate in the first 5 years and then declines rapidly. This is because the pressure variations resulted in early short-time miscible flooding and later immiscible flooding. The oil production rate in C1 are relatively stable and declined slowly with longer periods of high rates (Fig. 13b). The water cut in B3 declined quickly over the first 5 years to a minimum of 37.6% and then increased rapidly, the final value is higher than 95%, which may be resulted from the high injection pressure of B3. The water cut in C1 decrease over the first 10 years and then increase slowly in the last 10 years; the highest water cut is approximately 91% (Fig. 13c). The recovery factor of C1 shows an approximately linear trend, the B3 shows a quick increase and with a higher factor in early stage and decrease in last 5 years (Fig. 13d). The cumulative CO_2 stored in scenario B3 is only 3.8 $\times 10^6$t, which is the lowest of the three scenarios. In contrast, scenarios A2 and C1 have larger amounts of CO_2 stored (5.26 $\times 10^6$t for A2 and 4.92 $\times 10^6$t for C1). Therefore, scenarios A2 and C1 are better than B3 because of the stable oil production rate and field pressures, low water cut and high amount of CO_2 stored. Furthermore, the amount of CO_2 stored and recovery factor of scenario C1 are slightly better than those of A2, which is probably because two injection wells are used in scenario C1.

4.2.4 Miscible CO_2 flooding

The average reservoir pressures in scenarios A3, C2 and C3 (4794psi, 4498psi and 4877psi, respectively, Table 7) during CO_2 flooding are all high than the *MMP*, these scenarios, therefore, are considered to be miscible flooding. The reservoir pressures in scenarios A3 and C3 are high than *MMP* in the whole process (Fig. 14a). The A3 and C3 have very similar pressure build-up curves with a wide stable pressure range, which could be more beneficial for miscible CO_2 flooding.

The oil production rate of C3 increases significantly and rapidly over the initial stage with two peak values (Fig.14b), A3 has one peak but with different arrival times behind the C3 which indicates they have different CO_2 break through time and mechanism. The curves of rate decline of scenarios A3 and B3 are also very similar as shown in Fig. 14b. The water cuts of them also similarly decline significantly and quickly over the first 4 years and up to lowest and then goes up slowly with complex fluctuation (Fig. 14c), which indicate that the CO_2 flooding have effectively reduced the water cut during EOR. The recovery factors in scenarios A3 and C3 show very similar trends (Fig. 14d), and C3 always has higher factor than A3. The cumulative CO_2 stored in C3 is up to 10.7$\times 10^6$t, which is larger than in scenarios C2 (8.0$\times 10^6$t) and A3 (8.7$\times 10^6$t).

Except for the average reservoir pressure (that of C2 is lower than those of A3 and C3 due to the lower injection pressure), the other parameters of scenarios A3 and C3, including the oil production rate, amount of CO_2 stored, water cut, recovery factor and average pressure, have very similar trends (Fig. 14), which indicates that the most stable displacement was achieved in the miscible flooding scenarios. At the end of CO_2 injection in scenario C3, the ultimate recovery factor is 57.9%, and more than 10 $\times 10^6$t CO_2 had been stored in reservoir. In scenario A3, the ultimate

recovery factor is 51.85%, and 8.7 $\times 10^6$t CO_2 had been stored, which are very similar to C3. Therefore, the optimum CO_2 miscible flooding scenario is C3 with two injection wells and A3 with the I1 well.

4.2.5 Comparison of reservoir operations in the different scenarios

In the No-CO_2 scenario, the ultimate recovery factor at the end of 20 simulation years is only 37.37%, whereas the recovery factors in the immiscible, near-miscible and miscible CO_2 flooding scenarios vary from 42.73 to 45.08%, 48.14 to 49.80% and 51.85 to 57.92%, respectively. The oil production and reservoir pressure are all increased obviously after CO_2 flooding, and the recovery factor is raised approximately 5~20% over the No-CO_2 scenario, which shows a significant potential of CO_2 flooding. The exchange ratios of CO_2 to crude oil varies from 3.6~8.4t_{CO2}/t_{oil}, which indicates that a large amount of CO_2 is needed to store for replacing crude oil. So the CO_2 flooding efficiency is low, but the CO_2 storage efficiency is higher. As shown in Fig. 15, the cumulative oil production and amount of CO_2 stored are always the highest in the miscible scenarios C3, C2 and A3 in the whole CO_2 injection process. Thus, the best operation for this reservoir is with I1 and/or I2 injection well and high injection pressure (5,500 psi and/or 6,000 psi).

The corrections between ultimate oil recovery factors and CO_2 stored volumes in all of the CO_2 flooding scenarios in our simulation shows that the three scenario groups of immiscible, near-miscible and miscible are arranged in order from the lower left to the upper right. These results indicate that the injection pressure and flooding mechanism play an important role for the CO_2 enhance recovery and storage efficiency, and C3 is the best operation no matter from EOR or storage (Fig. 16). For the single well injection scenarios, the recovery factor and the amount of CO_2 stored in the series A scenario (A1, A2 and A3) are increased greater than that in series B (Fig. 16). It suggests that the potential for CO_2-EOR is higher when the injector is I1 rather than I2. Because the reservoir heterogeneity in the region of well I2 are higher than those in the area of I1, which affect sweep and gas/oil ratio (GOR). So the region of well I1 located are better for CO_2 flooding. Thus, scenario A3 is the optimization design for single well injection operations.

As mentioned previously, the optimum operations for single well injection and two well injections were scenarios A3 and C3, respectively. Therefore, these scenarios were selected and compared with the No-CO_2 in Fig. 17. The results show that the increases in the recovery factor and oil production and decreases in water cut are very similar, and the differences of ultimate recovery factor and cumulative CO_2 stored between the final results in A3 and C3 are very limited (<10%), which indicates that although the number of CO_2 injection wells has a significant effect on the reservoir behaviour and result during CO_2 flooding, they are not directly proportional. The reservoir properties of the injection region maybe the critical factor. The best scenario for M10 reservoir is high injection pressure operations with one injection well in region of I1 located if considering economic factors of offshore well and operation costs. However, the locations and numbers of CO_2 injection wells in these scenarios should be studied further considering other factors, such as the cost, gas oil ratio and CO_2 utilization efficiency.

4.3 Limitations and future work

This study has several limitations due to the limited available data from oilfield exploration and production, and these limitations are discussed here for further improvements in future studies. Firstly, several parameters in the quick screening model are based on simple calculations or experiential values. In addition, the model of the screening method is based on the sandstone oilfields in the Gulf of Mexico. Although the HZ21-1 field is also a marine sandstone oilfield, there are differences in the reservoir and fluid properties, particularly the bottom water activities. These may cause some errors or uncertainties. Secondly, most parameters used in the reservoir M10 modelling and simulation are from published data. The production history is only available through the end of 2005. Only 6 well logs, which were concentrated in the northern M10 reservoir, were collected to define the geological and compositional model. The oil components were obtained by fitting the properties.

For these limitations, we consider this study to be a preliminary attempt to the potential for CO_2-EOR and CO_2 storage in the oil reservoirs of the HZ21-1 field. The results of quick screening in this paper are generally consistent with previous qualitative analyses and did not generate any unexpected questions. The CO_2 flooding mechanism, EOR efficiency, CO_2 storage potential and injection-production design in the M10 oil reservoir have been conducted for the first time through reservoir modelling and compositional simulations. The results can be considered a numerical simulation test and preliminary evaluation of the CO_2-EOR and CO_2 storage potential as of the end of 2005 (data deadline), which helped to gain experience and provide a basis for future detailed evaluation studies. When additional data are available, future work might be focused on two aspects: 1) To build a quick screening model for the PRMB based on real data from the reservoirs of the basin; 2) To develop a better and more reliable numerical model of CO_2-EOR and storage that includes all reservoirs in the HZ21-1 and other oilfields in the basin.

5. Conclusion

HZ21-1 oilfield, characterized by high porosity, high permeability and light crude oil, has better geological conditions for CO_2 flooding. In this paper, the potential of CO_2-EOR and storage in reservoirs of the HZ21-1 oilfield has been evaluated through a workflow coupling site screening and numerical simulation methods. The reservoir pressure of HZ21-1 oilfield is a little less than *MMP,* so the CO_2 injection should be needed to increase the formation pressure so as to have a miscible flooding. The reservoir pressure and temperature are all lager than critical point of supercritical CO_2, thus the CO_2 sequestration mechanism should be in supercritical state.

Among reservoirs of HZ21-1 field, the L60 and M10 layers have the greatest potential for CO_2 flooding, followed by L40up, L50, L30 and L40low. Meanwhile, the potential of CO_2 storage can reach 0.8*PV*. The optimum operation for CO_2 injection into M10 should be set well pattern in region of injector I1 and higher injection bottom pressure for miscible flooding, which could take considerable EOR and storage potential with enhanced recovery factor of 20% and CO_2 stored mass of 10.7×10^6t CO_2. These injection scheme and potential assessment results could be extended to other reservoirs of HZ 21-1 oilfield. The HZ21-1 oilfield, therefore, should have a good EOR and storage potential

for applying the CO_2 flooding. In a word, although the reservoirs of HZ21-1 oilfield are small in scale, they are also suitable for CO_2 flooding and CO_2 geological storage, and the field can be used as candidate geological site for GDCCUS project.

As this study was based on published data, we are fully aware that the optimization operation is rather general and hypothetic. The model need to be revised over the entire HZ21-1 oilfield based on more detailed field data of reservoir characteristics, fluid properties and production history, so that the research results can guide and support the fulfilment of the CCUS development offshore Guangdong.

Acknowledgements

We gratefully acknowledge the funding provided by the open funds of State Key Laboratory of Oil and Gas Reservoir Geology and Exploitation (Chengdu University of Technology) (No. PLC20180801) and Guangdong Research Center for Unconventional Energy Engineering Technology (Guangdong University of Petrochemical Technology) (No. GF2018A009), the National Natural Science Foundation of China (No. 41372256) and the Natural Science Foundation of Guangdong Province, China (No. 2018A030313433). Two reviewers are thanked for their comments which significantly improved this manuscript.

References

Aminu, M.D., Nabavi, S.A., Rochelle, C.A., Manovic, V., 2017. A review of developments in carbon dioxide storage. Applied Energy 208, 1389-1419.

Azzolina, N.A., Nakles, D.V., Gorecki, C.D., Peck, W.D., Ayash, S.C., Melzer, L.S., Chatterjee, S., 2015. CO_2 storage associated with CO_2 enhanced oil recovery: A statistical analysis of historical operations. International Journal of Greenhouse Gas Control 37, 384-397.

Bi, F., Li, F., Liang, H., 2011. Domestic and Foreign Research and Application Progress on CO_2-EOR Technology. Value Engineering 06, 206-207 (in Chinese with English abstract).

Chen, J., Shi, H., Shu, Y., Du, J., Xie, T., 2007. The application of seal evaluation method with log data in Zhu Ⅰ depression, Pearl River Mouth basin. China Offshore Oil and Gas 19, 157-161.

Chen, W., Du, J., Long, G., Chen, S., Li, X., Zhang, S., Zhang, C., 2012. Factors controlling sanbody development and models of stratigraphic-lithologic traps of Zhujiang Formation in Huizhou area, Pearl River Month Basin. Oil and Gas Geology 33, 449-458 (in Chinese with English abstract).

DiPietro, P., Kuuskraa, V., Malone, T., 2015. Taking CO_2 enhanced oil recovery to the offshore Gulf of Mexico: A screening-level assessment of the technically and economically recoverable resource. SPE Economics & Management Jan. 2015, 3-9.

Du, Z., Zhang, R., 2000. Calculation of reservoir permeability using log data and lithofacies. Well Log technology 24, 521-523 (in Chinese with English abstract).

Fertl, W.H., Frost, E., Jr., 1980. Evaluation of Shaly Clastic Reservoir Rocks. SPE-8450-PA 32, 1641 - 1646.

GCCSI, 2016. The global Status of CCS: 2016 Summary Report. Global CCS Institute, Canberra, p. 204.

Hao, M., Song, Y., 2010. Research status of CO_2-EOR. Drilling and Production Technology 33, 59-63 (in Chinese with English abstract).

Hendriks, C., Graus, W., Bergen, F.v., 2004. Global carbon dioxide storage potential and costs. Ecofys, Utrecht, pp. 1-59.

Huang, Y., Guo, H., Liao, C., Zhao, D., 2013. The Study on Prospect and Early Opportunities for Carbon Capture and Storage in Guangdong Province, China. Energy Procedia 37, 3221-3232.

Jiao, Z., Zhou, L., Gao, R., Luo, T., Wang, H., Heng, W., Fred, M., Ramsey, B., Scott, Q., 2014. Opportunity and Challenges of Integrated Enhanced Oil Recovery Using CO_2 Flooding with Geological CO_2 Storage in the Ordos Basin, China. Energy Procedia 63, 7761-7771.

Kang, P.-S., Lim, J.-S., Huh, C., 2016. Screening Criteria and Considerations of Offshore Enhanced Oil Recovery. Energies 9, 44.
Kuuskraa, V., Wallace, M., 2014. CO_2-EOR set for growth as new CO_2 supplies emerge. OIL & GAS JOURNAL 112, 92-105.
Kuuskraa, V.A., Malone, T., 2016. CO_2 Enhanced Oil Recovery for Offshore Oil Reservoirs. Offshore Technology Conference.
Lei, X., Hu, Y., Liang, W., Liao, J., Liao, M., 2015. A study on sedimentary facies of oil group I in Member 2 of Zhujiang Formation in Wenchang 19-1 Oilfield. Journal of Southwest Petroleum University (Science & Technology Edition) 37, 1-12 (in Chinese with English abstract).
Li, P., Liu, X., Lu, J., Zhou, D., Hovorka, S., Hu, G., Liang, X., 2018. Potential evaluation of CO_2-EOR and storage in oilfields of Pearl River Mouth Basin, northern South China Sea. Greenhouse Gases: Science and Technology 8, 954-977.
Li, P., Zhou, D., Zhang, C., Zhang, Y., Peng, J., 2013. Potential of Sub-seafloor CO_2 Geological Storage in Northern South China Sea and its Importance for CCS Development in South China. Energy Procedia 37, 5191-5200.
Li, Q., Chen, Z.A., Zhang, J.T., Liu, L.C., Li, X.C., Jia, L., 2016. Positioning and Revision of CCUS Technology Development in China. International Journal of Greenhouse Gas Control 46, 282-293.
Li, Q., Wang, Q., Yu, X., Liang, W., Shui, M., 2008. A study on sedimentary microfacies of the shore facies reservoir in Lufeng 13-2 Oilfield. Journal of Oil and Gas Technology 30, 236-240 (in Chinese with English abstract).
Li, X., Zhou, D., Li, P., Wu, Y., Liang, X., Wei, N., Haszeldine, S., Senior, B., Shu, Y., Li, J., Chen, Y., 2015. CO_2 offshore Storage in China: Research Review and Plan for Demonstration Project. UK-China (Guangdong) CCUS Centre, p. 46.
Liu, B., 2011. Development of Oil and Gas fields of China. Volume of oil and gas fields in eastern South China Sea. Edited by editorial committee of "Development of Oil and Gas fields of China". Petroleum Industry Press, Beijing.
Liu, H., Gao, S., 1995. Pilot field test in development of Daqing oilfield. Petroleum Industry Press, Beijing.
Liu, H.J., Were, P., Li, Q., Gou, Y., Hou, Z., 2017. Worldwide Status of CCUS Technologies and Their Development and Challenges in China. Geofluids 2017, 1-25.
Luo, E., Hu, Y., Li, B., Zhu, W., 2013. Practices of CO_2 EOR in China. Special oil and gas reservoirs 20, 1-9 (in Chinese with English abstract).
Malone, T., Kuuskraa, V., DiPietro, P., 2014. CO_2-EOR Offshore Resource Assessment. DOE/NETL, p. 100.
Mungan, N., 1992. Carbon dioxide flooding as an enhanced oil recovery process. Journal of Canadian Petroleum Technology 31, 13-15.
Qin, J., Han, H., Liu, X., 2015. Application and enlightenment of carbon dioxide flooding in the United States of America. Petroleum exploration and development 42, 209-216 (in Chinese with English Abstract).
Shaw, J., Bachu, S., 2002. Screening, evaluation, and ranking of oil Reservoirs suitable for CO_2-flood EOR and carbon dioxide sequestration. Journal of Canadian Petroleum Technology 41, 51-61.
Shen, P., Jiang, H., Chen, Y., Li, Y., Liu, J., 2007. EOR study of CO_2 injection. Special Oil and Gas Reservoirs 14, 1-4 (in Chinese with English abstract).
Shen, P., Liao, X., 2009. The technology of carbon dioxide stored in geological meida and enhanced oil recovery. Petroleum Industry Press, Beijing.
Shi, H., Li, W., Zou, X., Yu, X., 1999. A study on sedimentary facies of sandstone oil fields in eastern Pearl River Mouth Basin. China Offshore Oil and Gas 13, 181-188 (in Chinese with English abstract).
Timur, A., 1968. An investigation of permeability, porosity, and residual water saturation relationship for sandstone reservoirs. Log Analyst 9, 8-17.
Wang, S., Zhao, l., Lu, G., Liu, X., Chen, R., Zhang, Q., Zhang, Z., Jiao, D., 1990. Petroleum geology of oil & gas bearing area on continental shelf and its neighbouring regions, in: Zhai, G. (Ed.), Petroleum geology of China. Petroleum Industry Press, Beijing, pp. 343-450.
Wood, D.J., 2006. Creating a Quick Screening Model for CO_2 Flooding and Storage in Gulf Coast Reservoirs Using Dimensionless Groups. The University of Texas at Austin.
Zhai, G., Wang, S., 1990. Petroleum geology of China, Vol.16, Oil and gas bearing areas on the continental shelf and ints neighbouring regions. Petroleum Industry Press, Beijing.

Zhao, D.F., Liao, X.W., Yin, D.D., 2014. Evaluation of CO_2 enhanced oil recovery and sequestration potential in low permeability reservoirs, Yanchang Oilfield, China. Journal of the Energy Institute 87, 306-313.
Zhou, D., Li, P., Liang, X., Liu, M., Wang, L., 2018. A long-term strategic plan of offshore CO_2 transport and storage in northern South China Sea for a low-carbon development in Guangdong province, China. International Journal of Greenhouse Gas Control 70, 76-87.
Zhou, D., Liao, C., Li, P., Huang, Y., 2013a. CCS Can Make Fossil-Fueled Energy Clean in Guangdong Province, China. Advanced Materials Research 807-809, 783-789.
Zhou, D., Zhao, D., Liu, Q., Li, X.-C., Li, J., Gibbons, J., Liang, X., 2013b. The GDCCSR Project Promoting Regional CCS-Readiness in the Guangdong Province, South China. Energy Procedia 37, 7622-7632.
Zhou, D., Zhao, Z., Liao, J., Sun, Z., 2011. A preliminary assessment on CO_2 storage capacity in the Pearl River Mouth Basin offshore Guangdong, China. International Journal of Greenhouse Gas Control 5, 308-317.
Zhu, C., Chen, L., 2007. Research on CO_2 flooding in low permeability reservoir. Drilling and Production Technology 30, 55-57 (in Chinese with English abstract).
Zhu, W., Mi, L., Zhang, H., 2010. Atlas of oil and gas basins, China sea. Petroleum Industry Press Beijing.

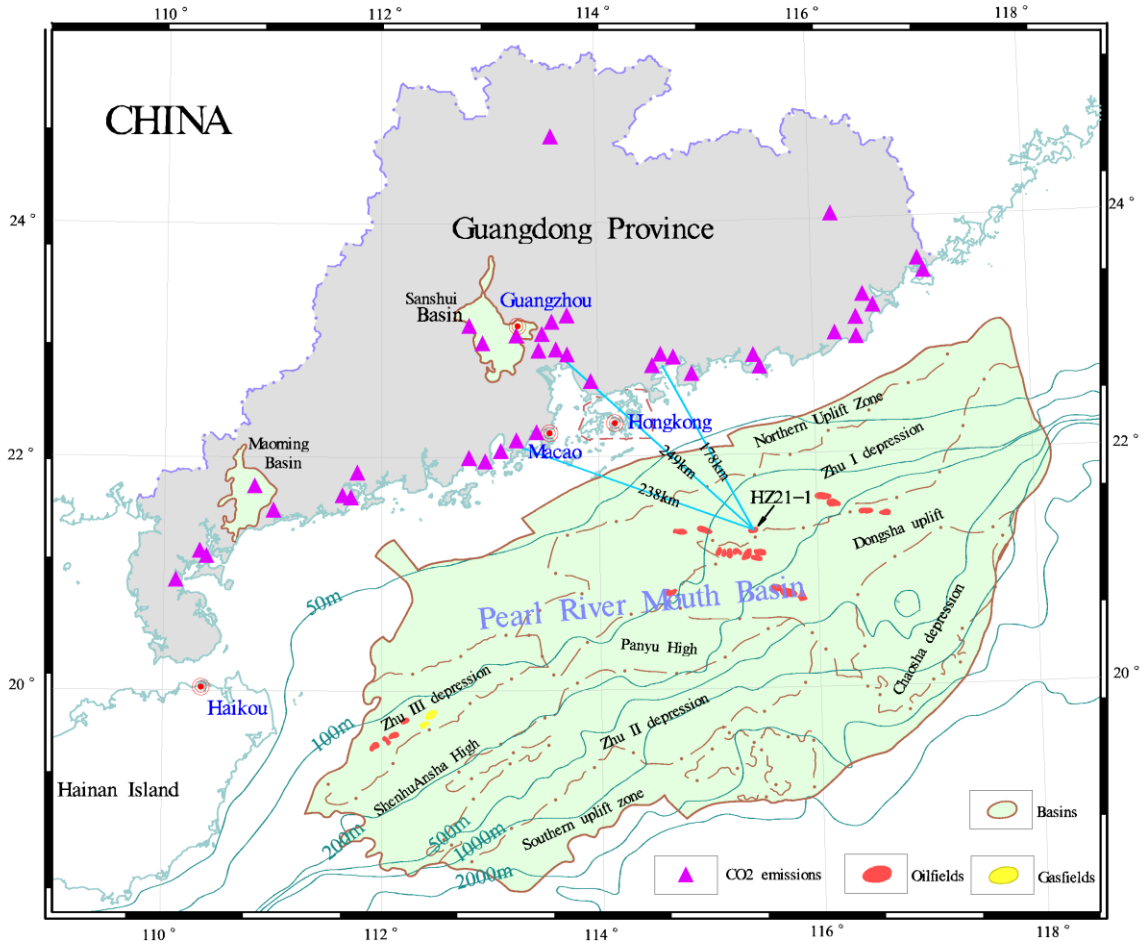

Fig. 1. Map of onshore and offshore sedimentary basins in and near Guangdong Province, large CO_2 point sources along the coast, and the locations of the HZ21-1 oil and gas field and other oil fields in the Pearl River Mouth Basin. The large CO_2 point sources along the coast are after (Huang et al., 2013), and the basin map is taken from (Zhu et al., 2010). The distances between several CO_2 point sources and the HZ21-1 field are also shown.

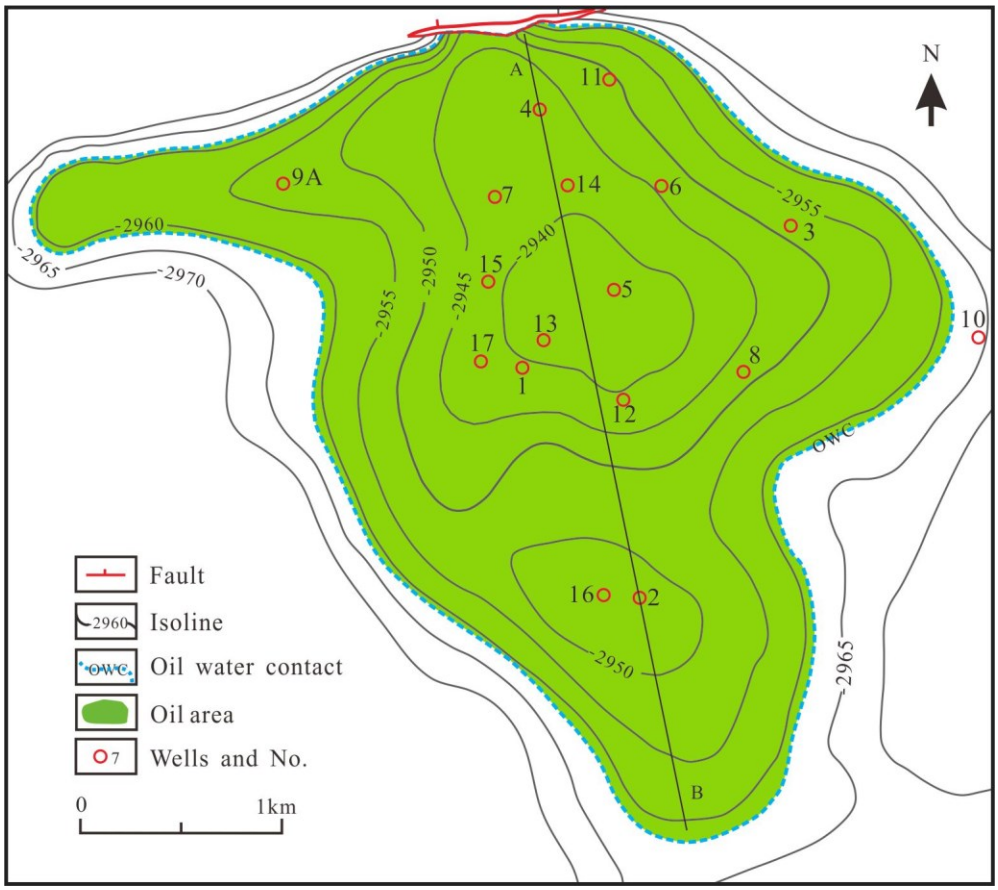

Fig. 2. Structure map of the HZ21-1 field showing depth contours of the top M10 reservoir. Depths are in metres, and the oil area, oil water contact and locations of the wells are also shown. Lin AB is the location of section in Fig.3. The data refers from Liu (2011) and Zhu et al. (2010).

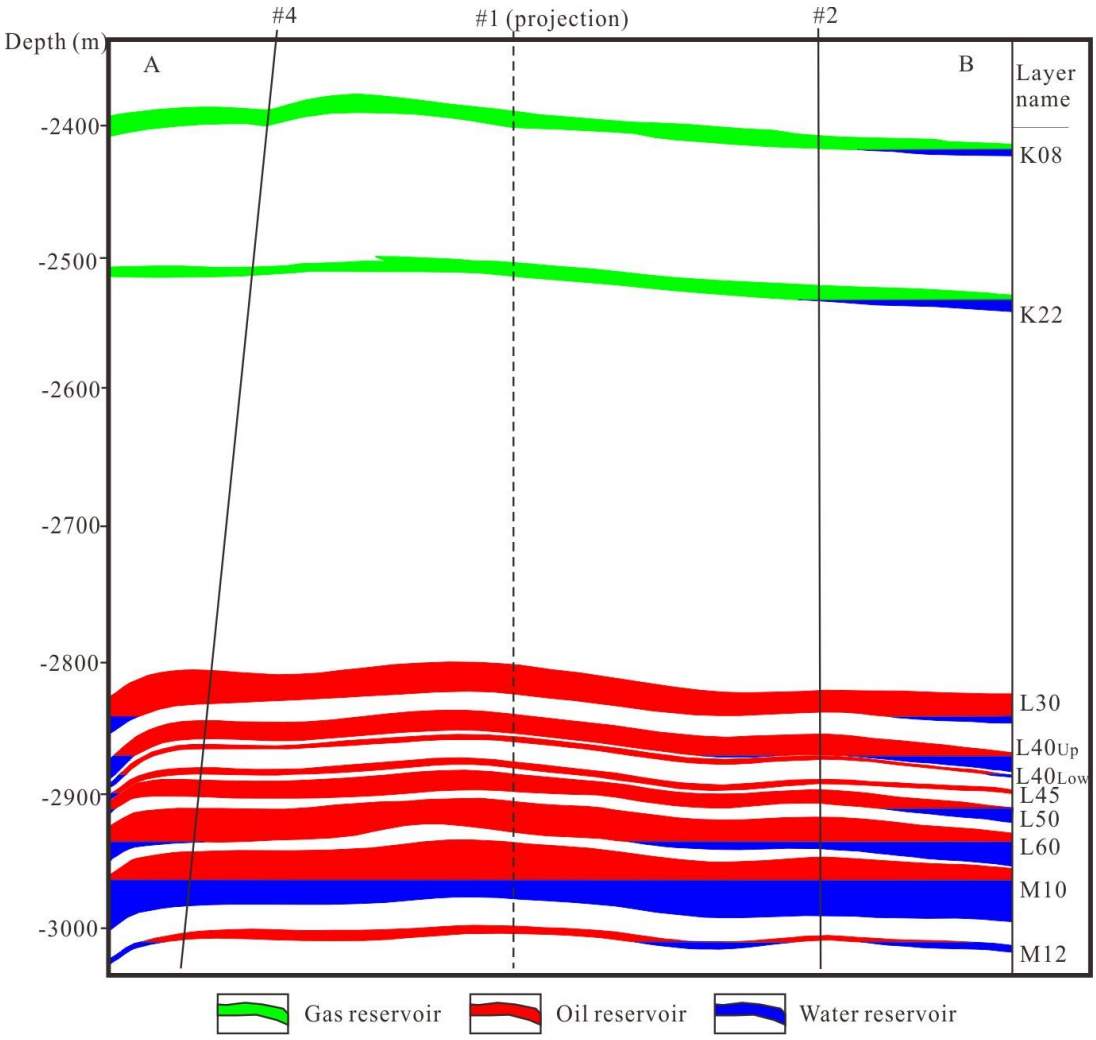

Fig. 3. N-S reservoir cross section of HZ21-1 field. Redrawn after Liu (2011) and Zhu et al. (2010). The line and well locations are shown in Fig. 2.

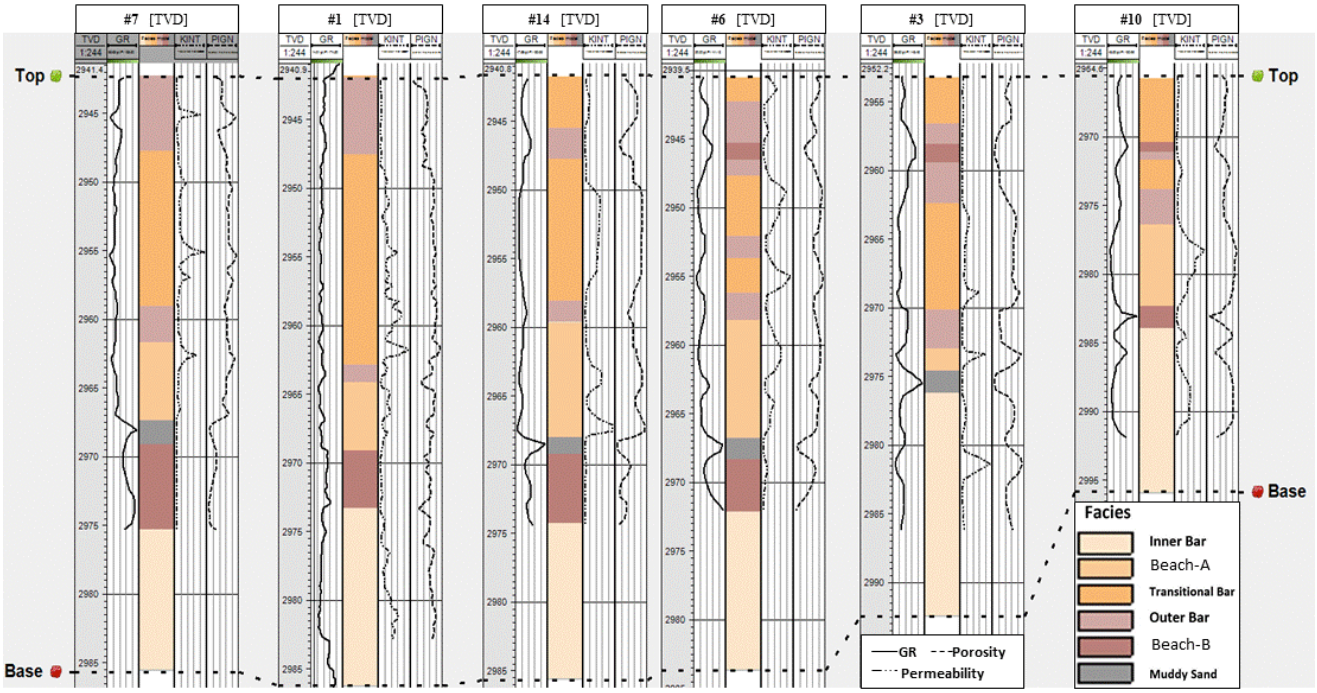

Fig. 4. Cross-well sections with well logs, lithofacies, porosities and permeabilities. The tracks for each well, from left to right, are gamma ray (GR), lithofacies, permeability, and porosity. The vertical scale is the depth in metres. These curves and the column of lithofacies were interpreted on the Petrel platform except for the GR curves (Liu, 2011), and the curves for the #1 well are courtesy of CNOOC Shenzhen.

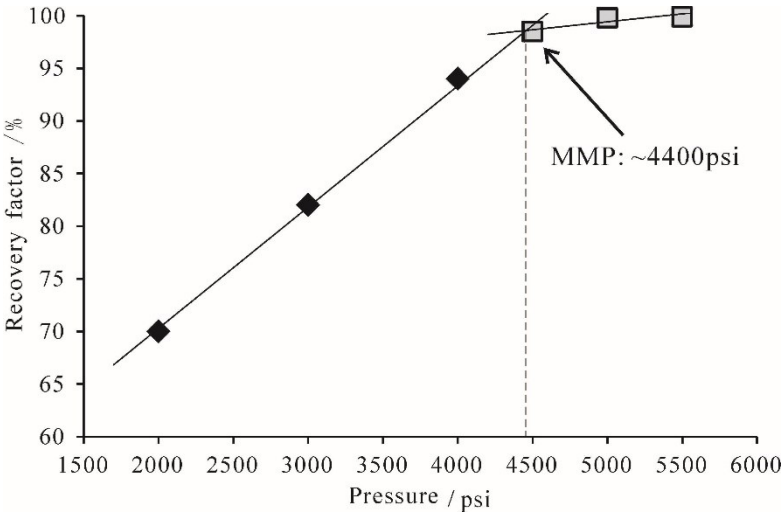

Fig. 5. Relationship between the oil recovery factor and injection pressure resulting from the slim tube simulation at 1.2 PV of CO_2 injection which shows the minimum miscible pressure (*MMP*) is ~4400 psi.

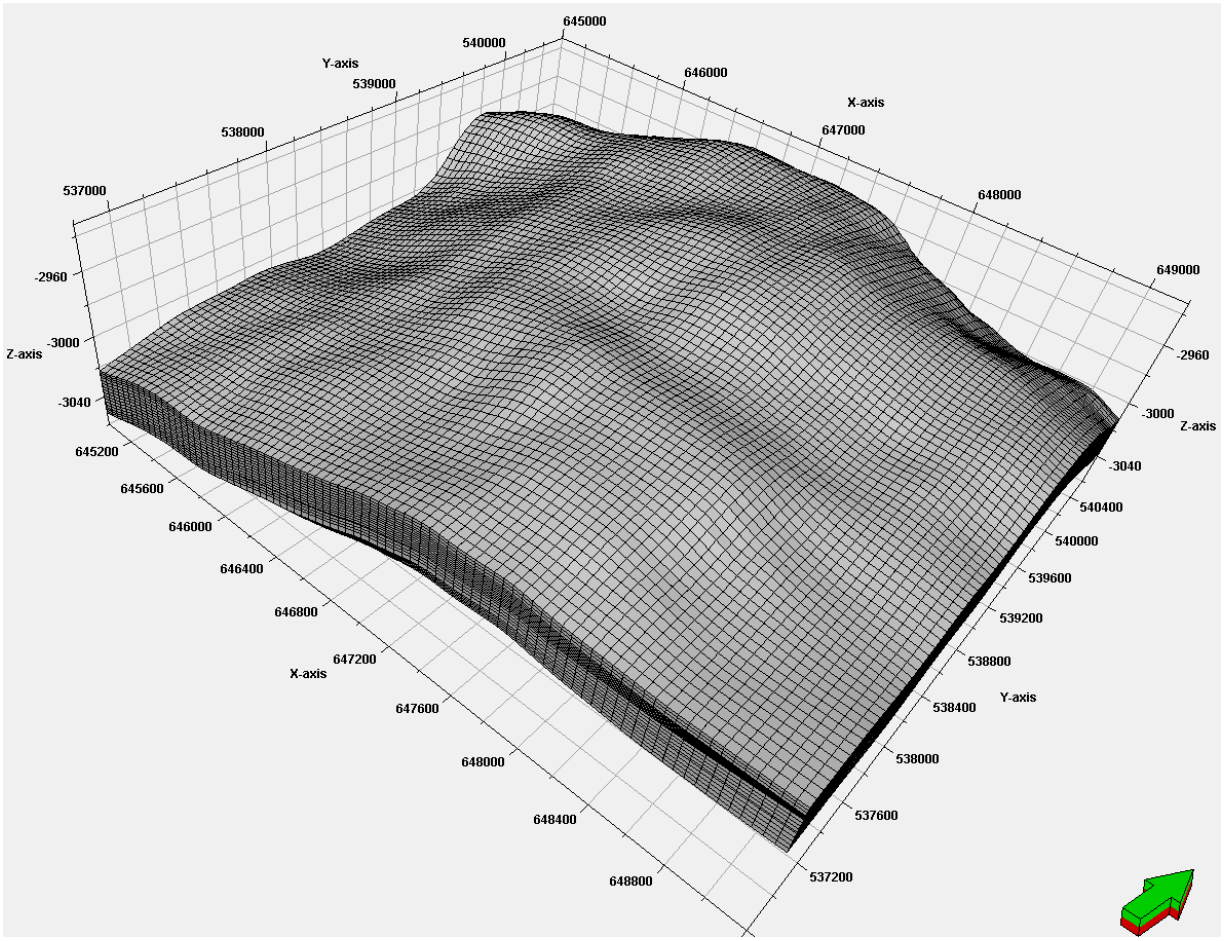

Fig. 6. Gridded model of the M10 reservoir with NX=84, NY=76, NZ=23, which is 4200 m long and 3800 m wide. The average thickness is 41.7 m.

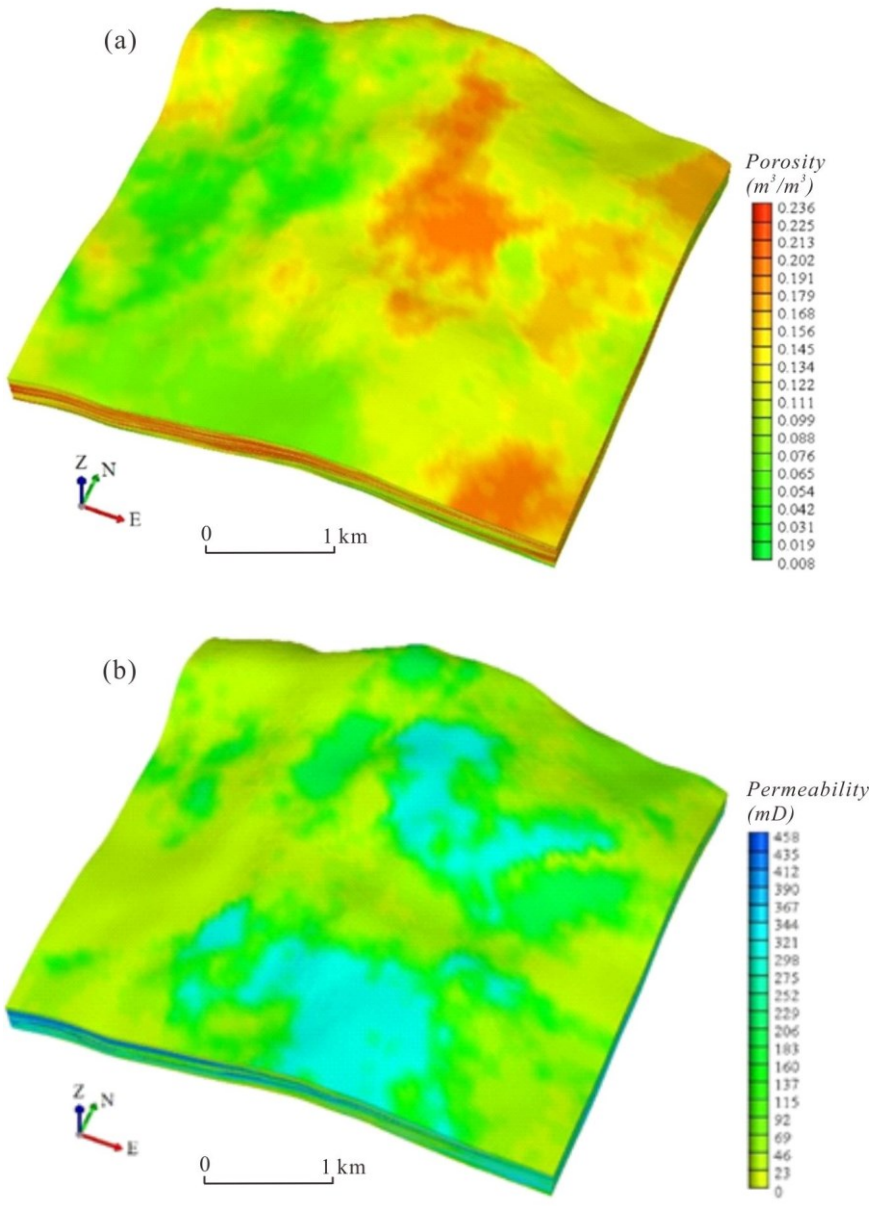

Fig. 7. 3D property models of porosity (a) and permeability (b) for the M10 reservoir. The vertical (z) exaggeration is 10 times.

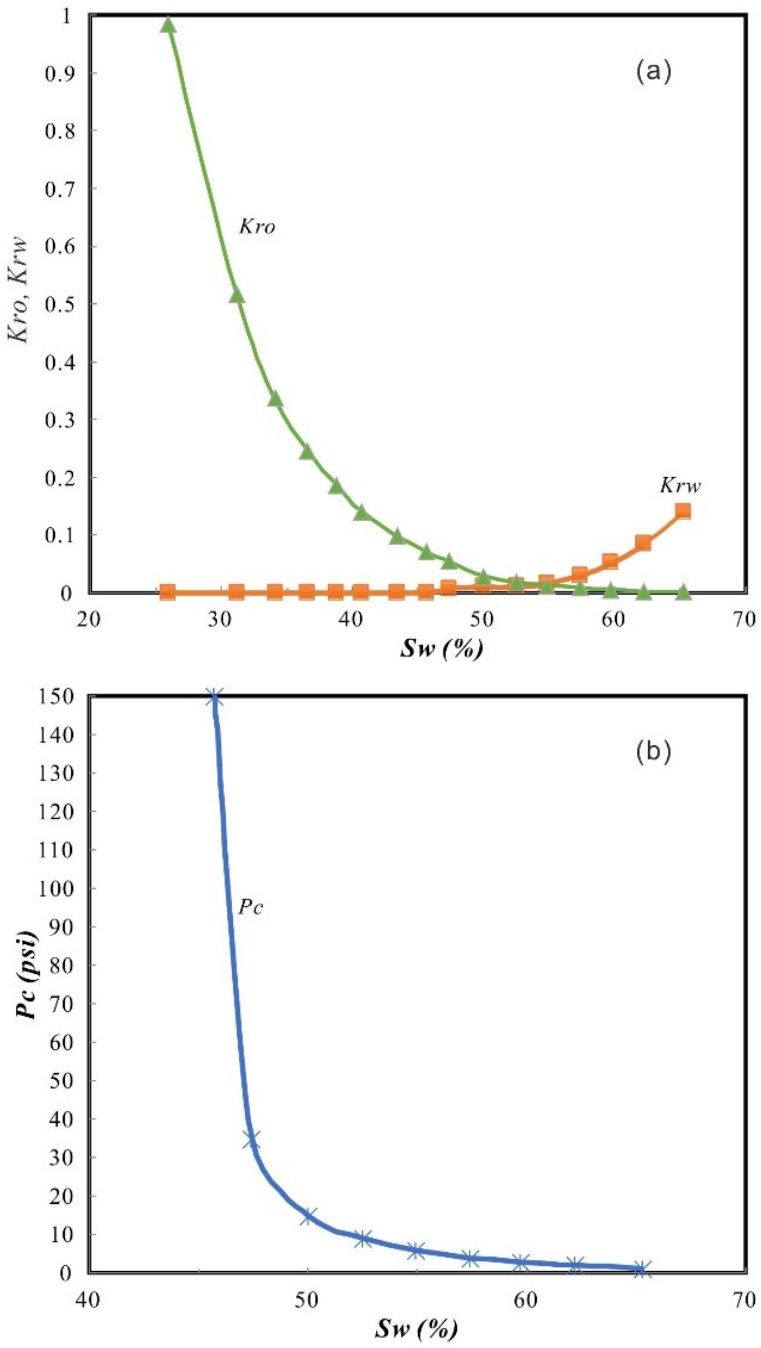

Fig. 8. Relative permeability (*Kr*) curves of the oil-water phases (a) and capillary pressure (*P*c) curve (b) based on field core data (refer from Liu (2011))

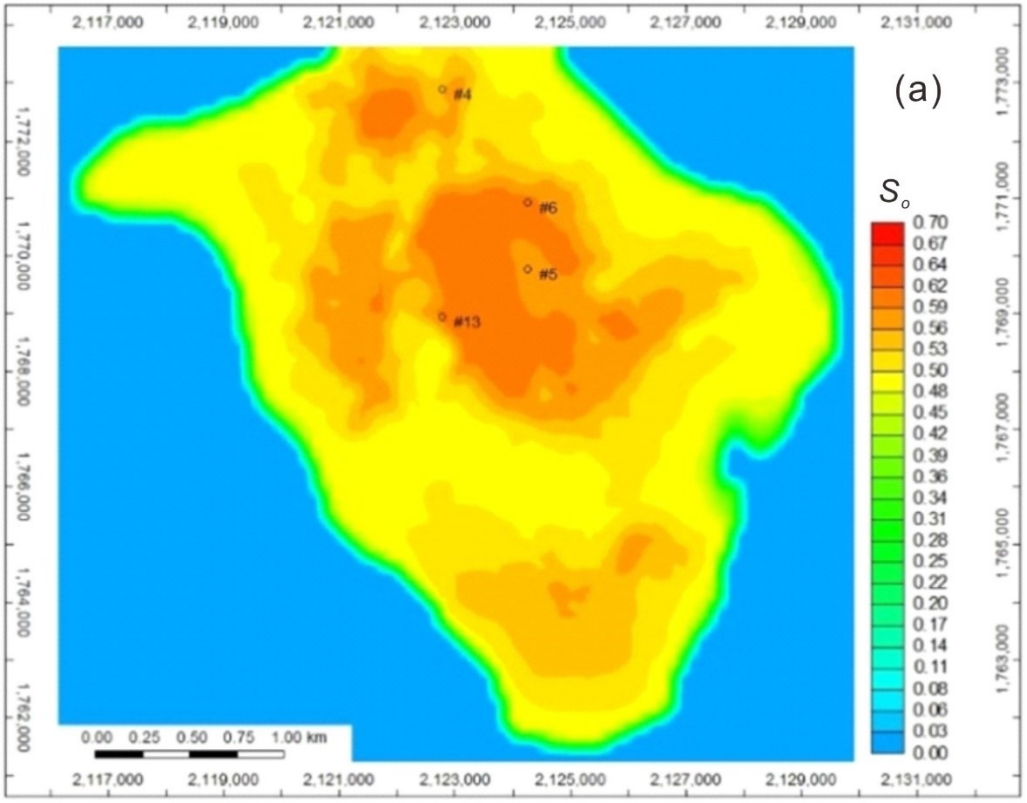
(a)
S_o
0.70
0.67
0.64
0.62
0.59
0.56
0.53
0.50
0.48
0.45
0.42
0.39
0.36
0.34
0.31
0.28
0.25
0.22
0.20
0.17
0.14
0.11
0.08
0.06
0.03
0.00
#4
#6
#5
#13
0.00 0.25 0.50 0.75 1.00 km
2,117,000
2,119,000
2,121,000
2,123,000
2,125,000
2,127,000
2,129,000
2,131,000
1,772,000
1,770,000
1,768,000
1,766,000
1,764,000
1,762,000
1,773,000
1,771,000
1,769,000
1,767,000
1,765,000
1,763,000

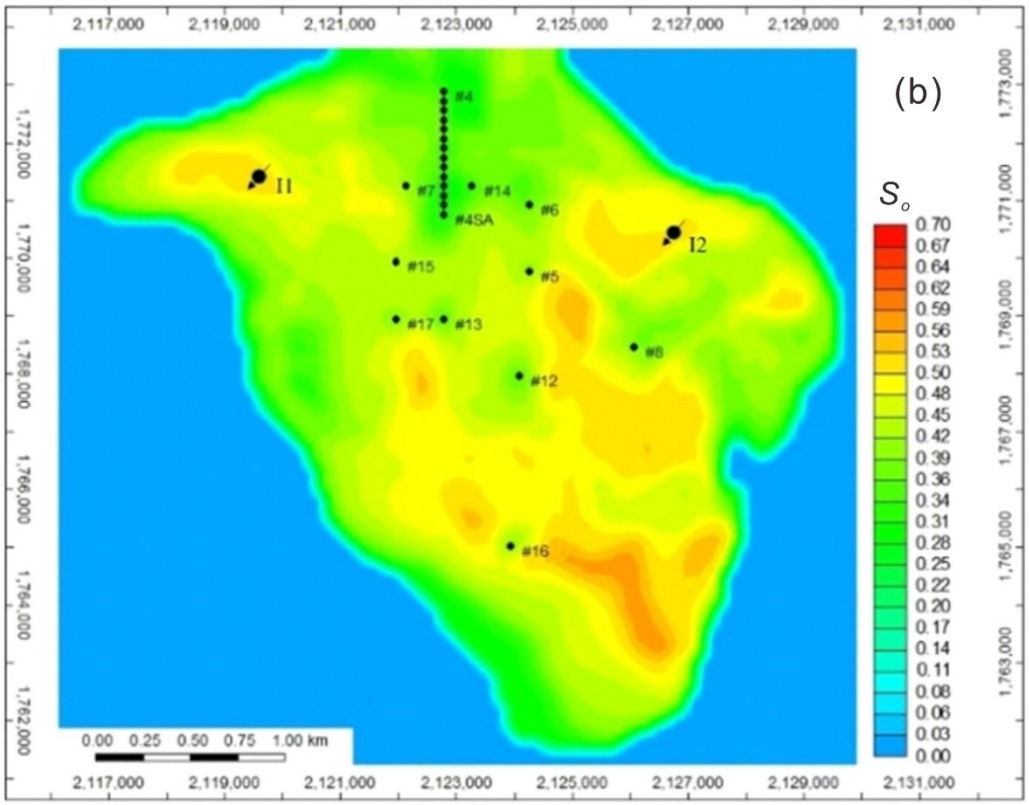
(b)
S_o
0.70
0.67
0.64
0.62
0.59
0.56
0.53
0.50
0.48
0.45
0.42
0.39
0.36
0.34
0.31
0.28
0.25
0.22
0.20
0.17
0.14
0.11
0.08
0.06
0.03
0.00
I1
I2
#4
#7
#14
#6
#4SA
#15
#5
#17
#13
#8
#12
#16
0.00 0.25 0.50 0.75 1.00 km
2,117,000
2,119,000
2,121,000
2,123,000
2,125,000
2,127,000
2,129,000
2,131,000
1,772,000
1,770,000
1,768,000
1,766,000
1,764,000
1,762,000
1,773,000
1,771,000
1,769,000
1,767,000
1,765,000
1,763,000

Fig. 9. Modelled oil saturation (S_o) distributions: (a) in 1990 when field was discovered; (b) in 2016 at the start of CO_2 injection. The black dots are oil production wells, and the dots with arrows are CO_2 injection wells.

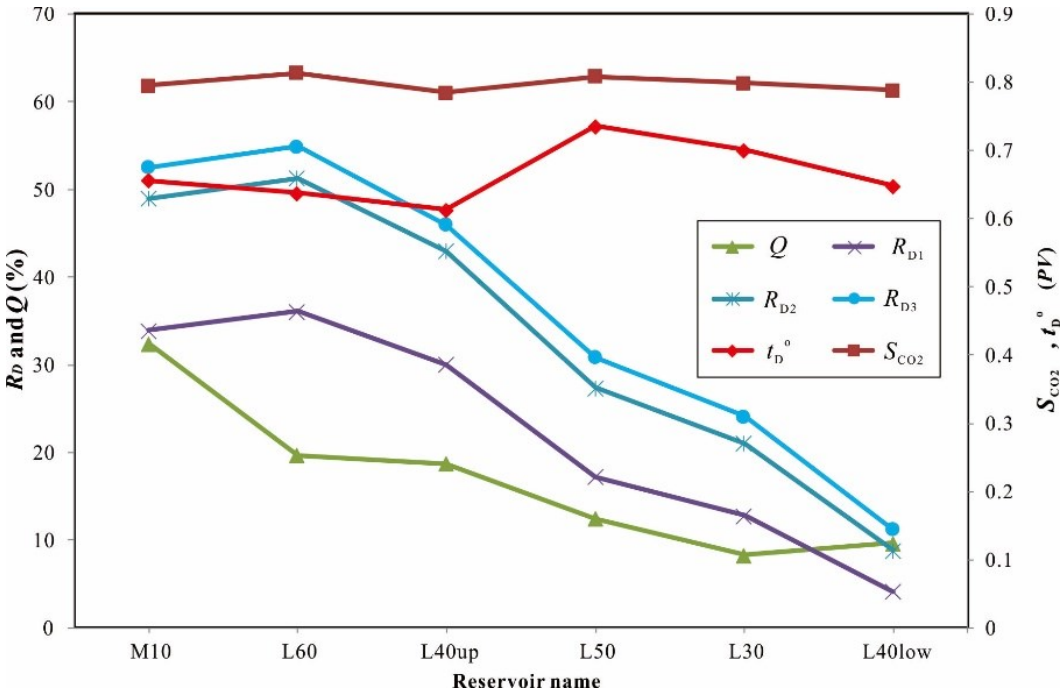

Fig. 10. Trend curves of resulted dimensionless outputs (t_D^0, R_{D1}, R_{D2}, R_{D3}, S_{CO2}) of the quick screening model for 6 oil reservoirs in the HZ21-1 field (revised based on Li et al. (2018)). The reserves ratios (Q) are also shown for comparison analysis.

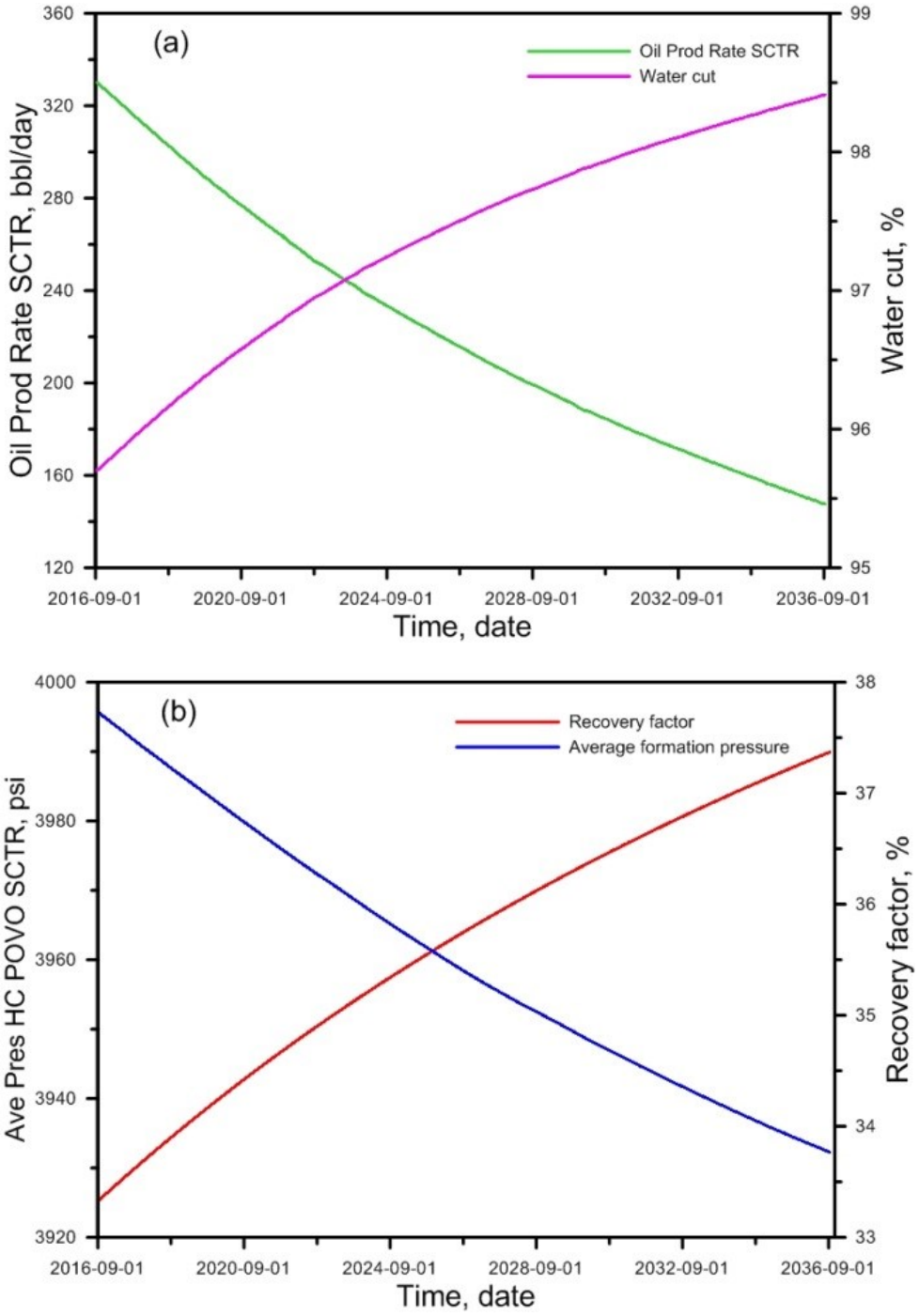

Fig. 11. Simulated curves of oil production rate and water cut (a) and oil recovery factor and average reservoir pressure (b) during primary production in the No-CO_2 scenario.

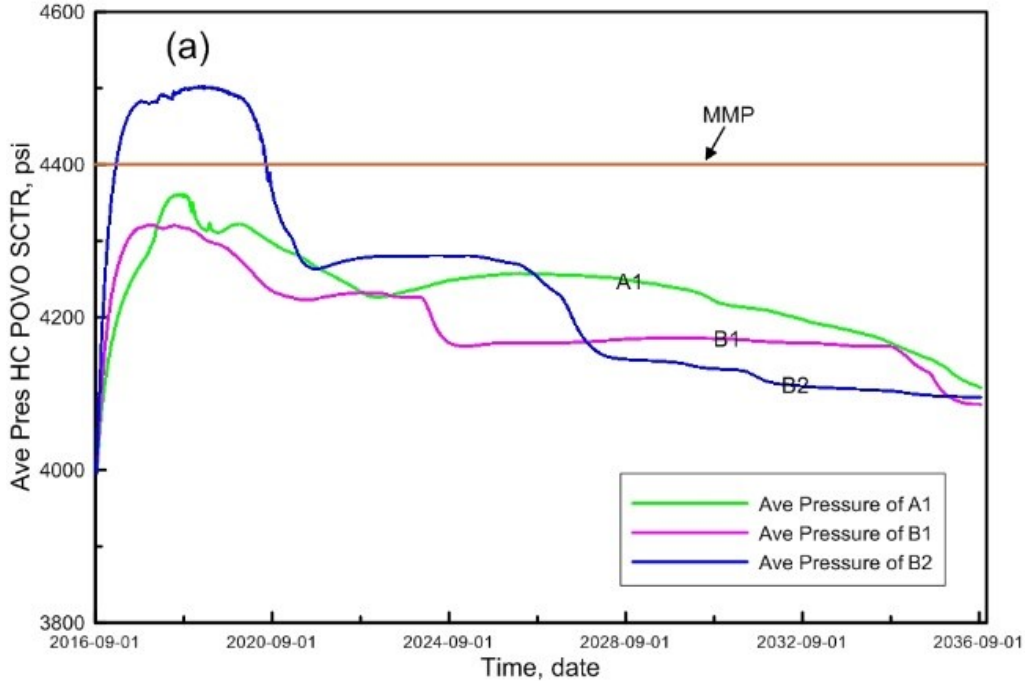
(a)
MMP
A1
B1
B2
Ave Pressure of A1
Ave Pressure of B1
Ave Pressure of B2
Ave Pres HC POVO SCTR, psi
Time, date
4600
4400
4200
4000
3800
2016-09-01
2020-09-01
2024-09-01
2028-09-01
2032-09-01
2036-09-01

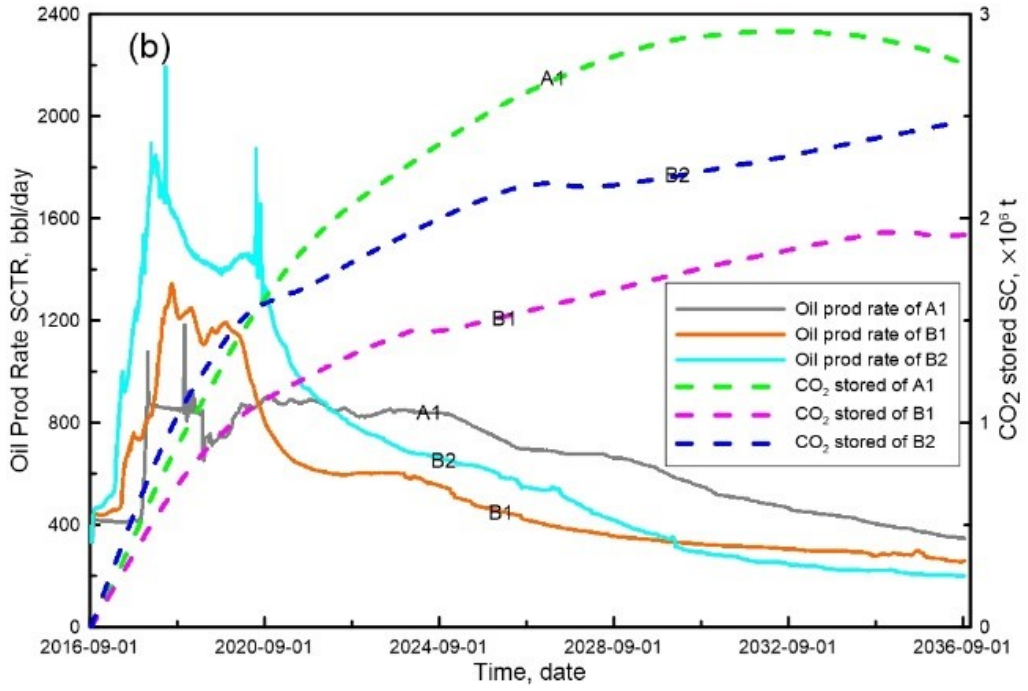
(b)
A1
B2
B1
A1
B2
B1
Oil prod rate of A1
Oil prod rate of B1
Oil prod rate of B2
CO2 stored of A1
CO2 stored of B1
CO2 stored of B2
Oil Prod Rate SCTR, bbl/day
CO2 stored SC, ×10⁶ t
Time, date
2400
2000
1600
1200
800
400
0
3
2
1
0
2016-09-01
2020-09-01
2024-09-01
2028-09-01
2032-09-01
2036-09-01

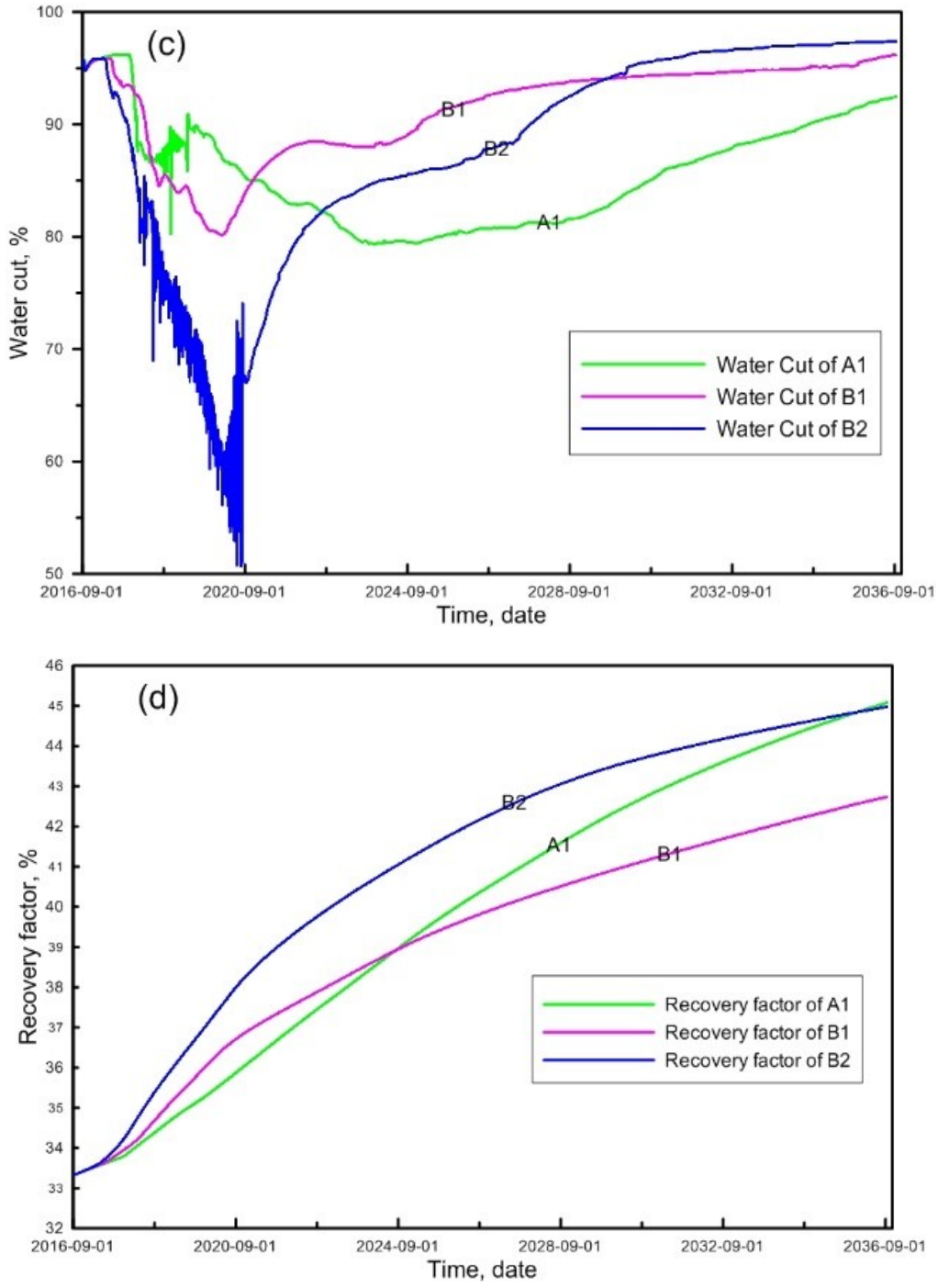

Fig. 12. Simulated curves of average reservoir pressure (a), oil production rate and CO_2 stored mass (b), water cut (c) and oil recovery factor (d) during the CO_2 flooding of scenarios A1, B1 and B2.

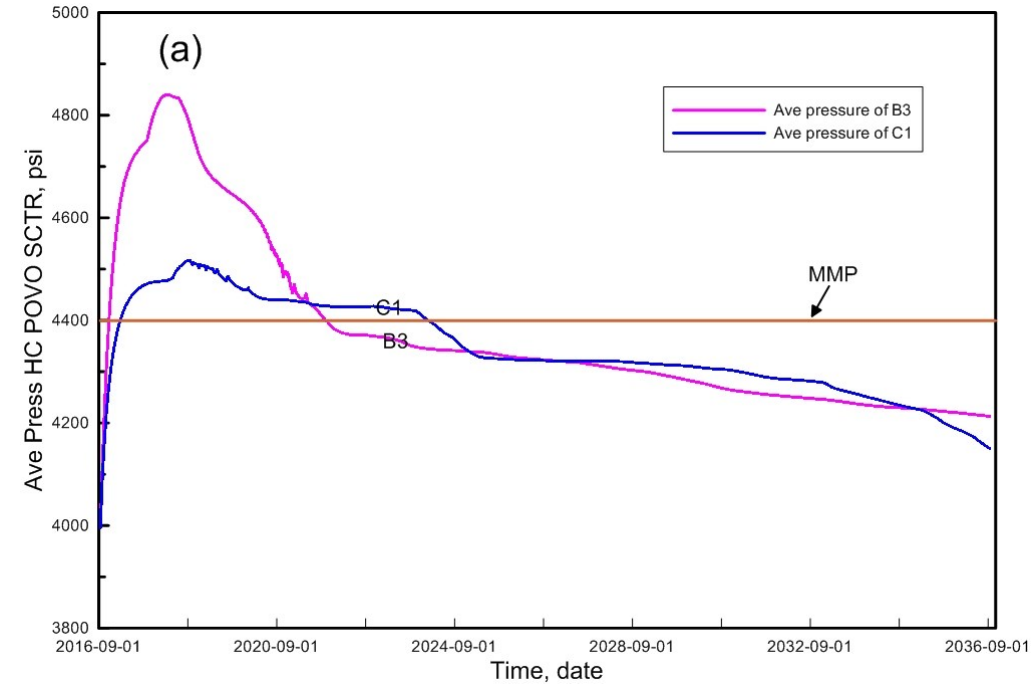
(a)
Ave pressure of B3
Ave pressure of C1
MMP
C1
B3
Ave Press HC POVO SCTR, psi
Time, date
5000
4800
4600
4400
4200
4000
3800
2016-09-01
2020-09-01
2024-09-01
2028-09-01
2032-09-01
2036-09-01

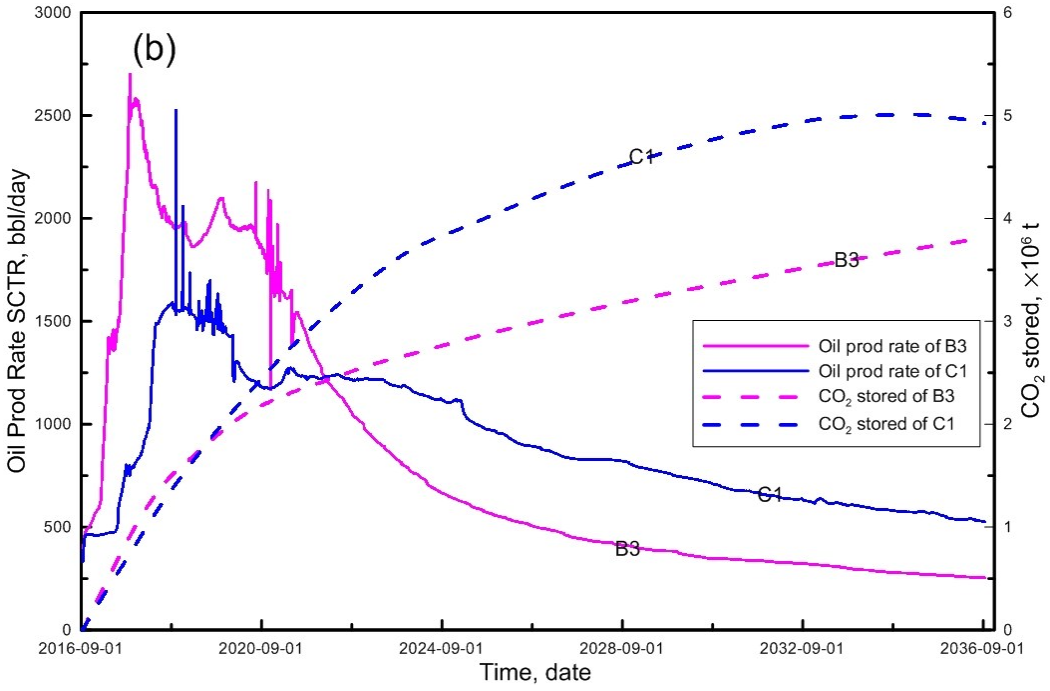
(b)
Oil prod rate of B3
Oil prod rate of C1
CO2 stored of B3
CO2 stored of C1
C1
B3
C1
B3
Oil Prod Rate SCTR, bbl/day
CO2 stored, ×10^6 t
Time, date
3000
2500
2000
1500
1000
500
0
6
5
4
3
2
1
0
2016-09-01
2020-09-01
2024-09-01
2028-09-01
2032-09-01
2036-09-01

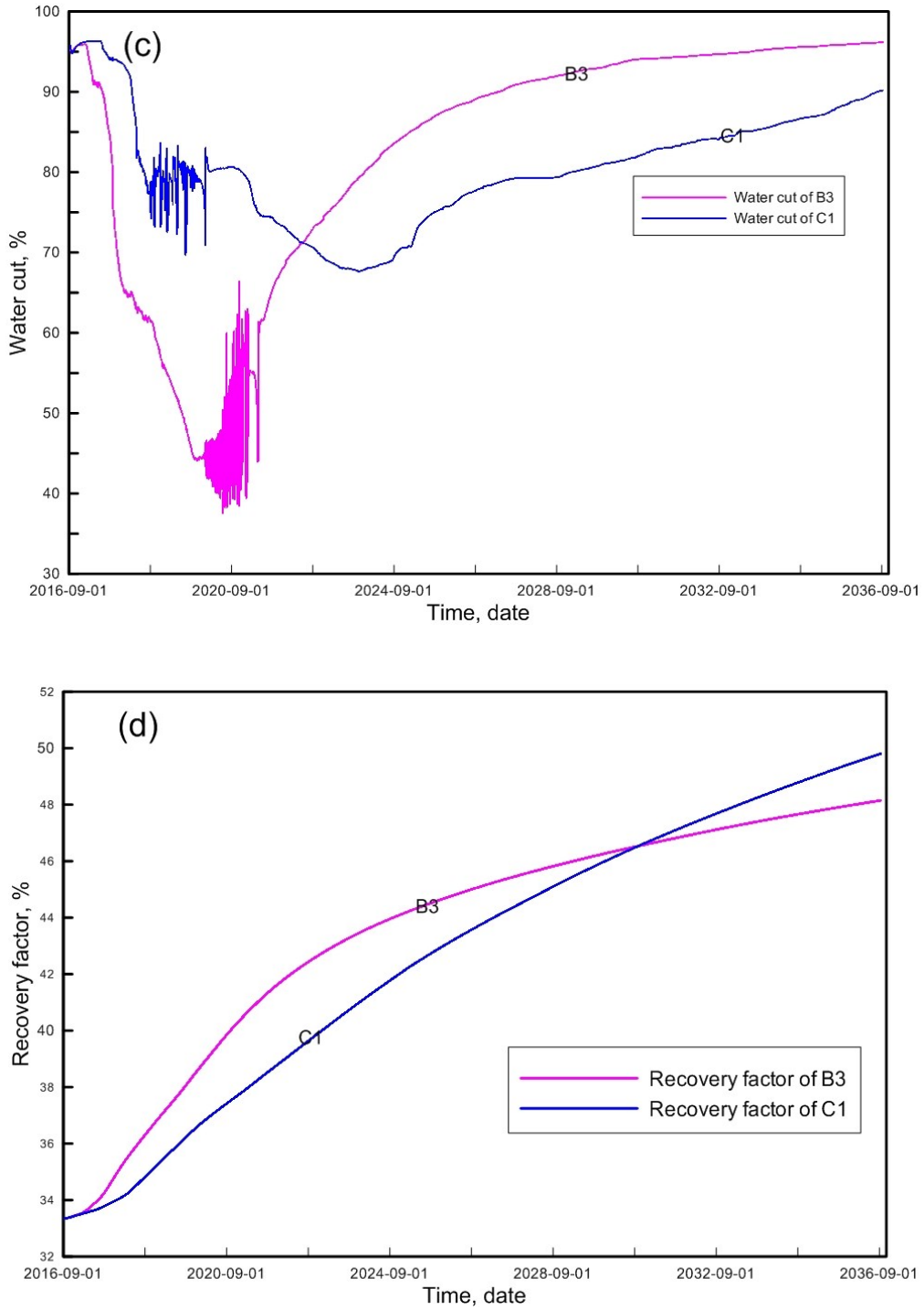

Fig. 13. Simulated curves of average reservoir pressure (a), oil production rate and CO_2 stored mass (b), water cut (c) and oil recovery factor (d) during the CO_2 flooding of scenarios B3 and C1.

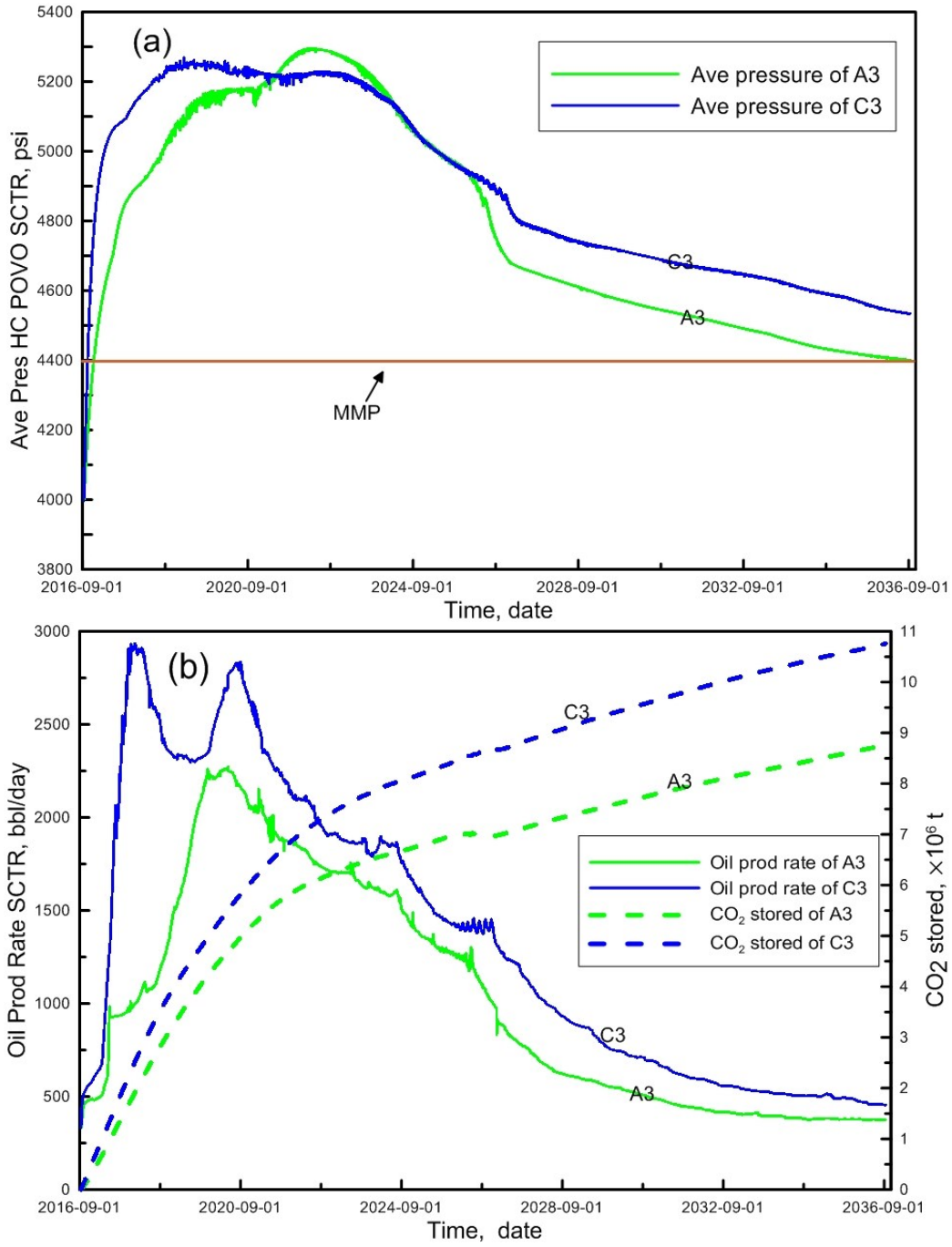
(a)
Ave pressure of A3
Ave pressure of C3
C3
A3
MMP
Ave Pres HC POVO SCTR, psi
Time, date
5400
5200
5000
4800
4600
4400
4200
4000
3800
2016-09-01
2020-09-01
2024-09-01
2028-09-01
2032-09-01
2036-09-01
(b)
Oil prod rate of A3
Oil prod rate of C3
CO2 stored of A3
CO2 stored of C3
C3
A3
C3
A3
Oil Prod Rate SCTR, bbl/day
CO2 stored, ×10^6 t
Time, date
3000
2500
2000
1500
1000
500
0
11
10
9
8
7
6
5
4
3
2
1
0

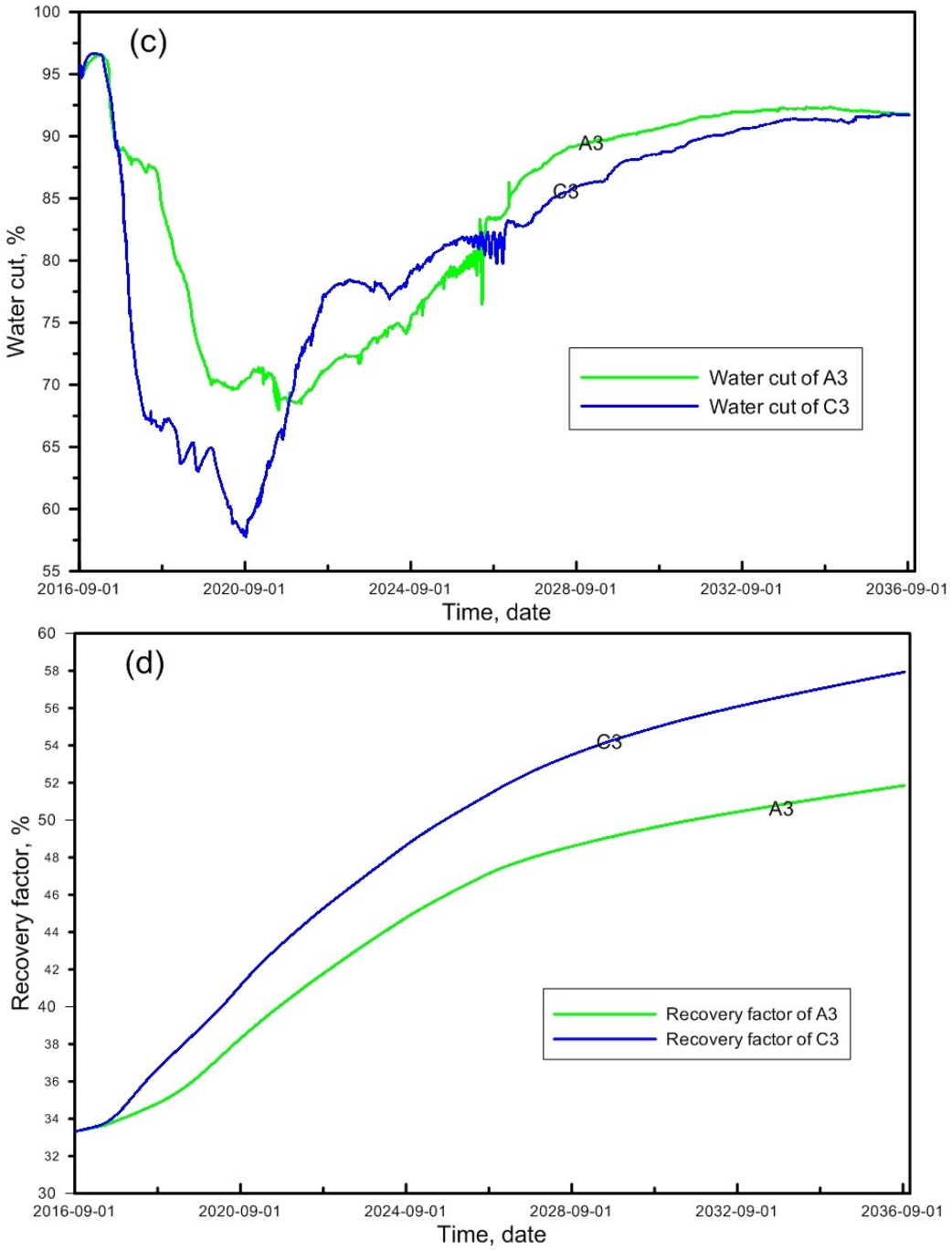

Fig. 14. Simulated curves of average reservoir pressure (a), oil production rate and CO_2 stored mass (b), water cut (c) and oil recovery factor (d) of during the CO_2 flooding of scenarios A3 and C3.

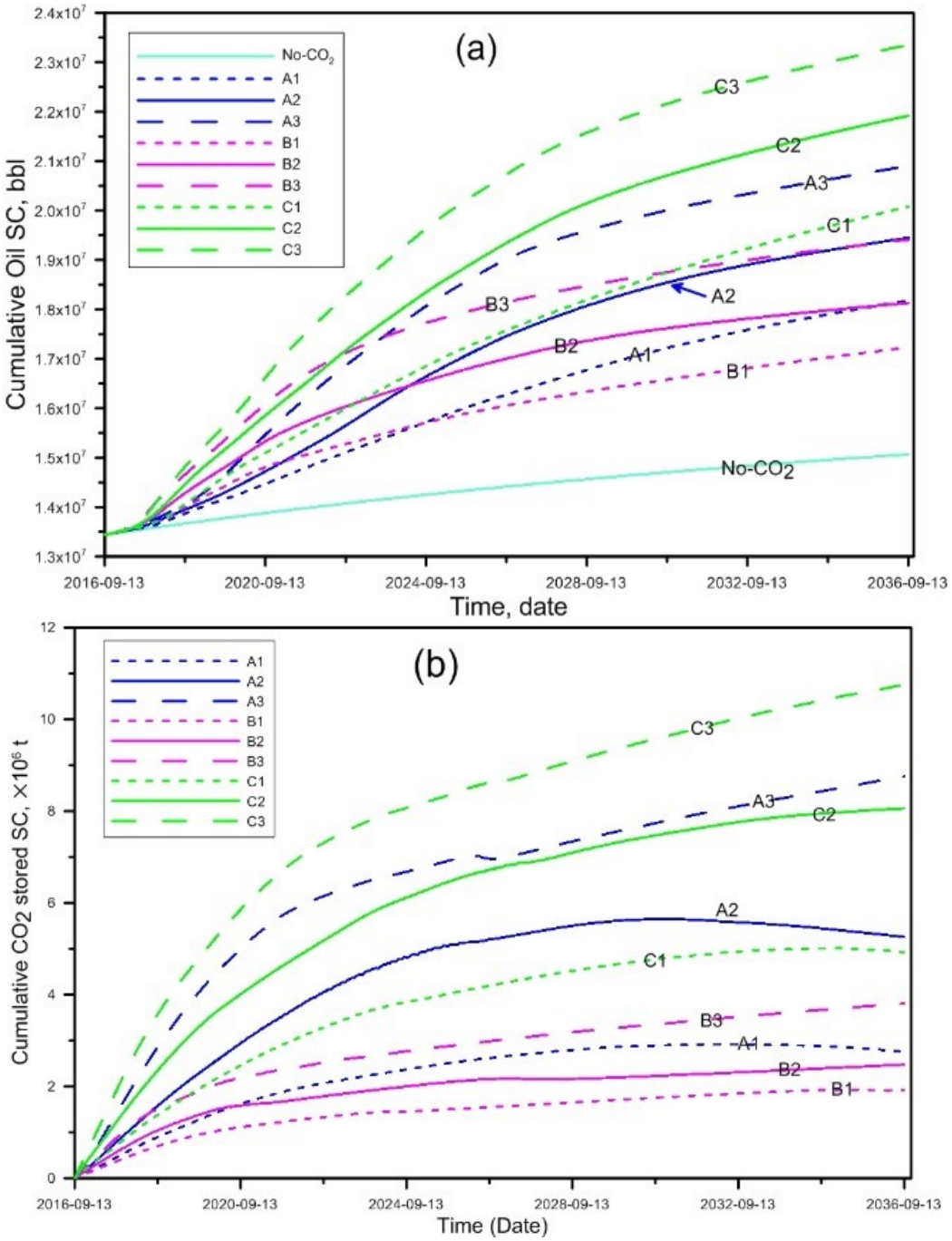

Fig. 15. Simulated curves of cumulative oil production (a) and cumulative CO_2 storage (b) over time for the scenarios in simulation.

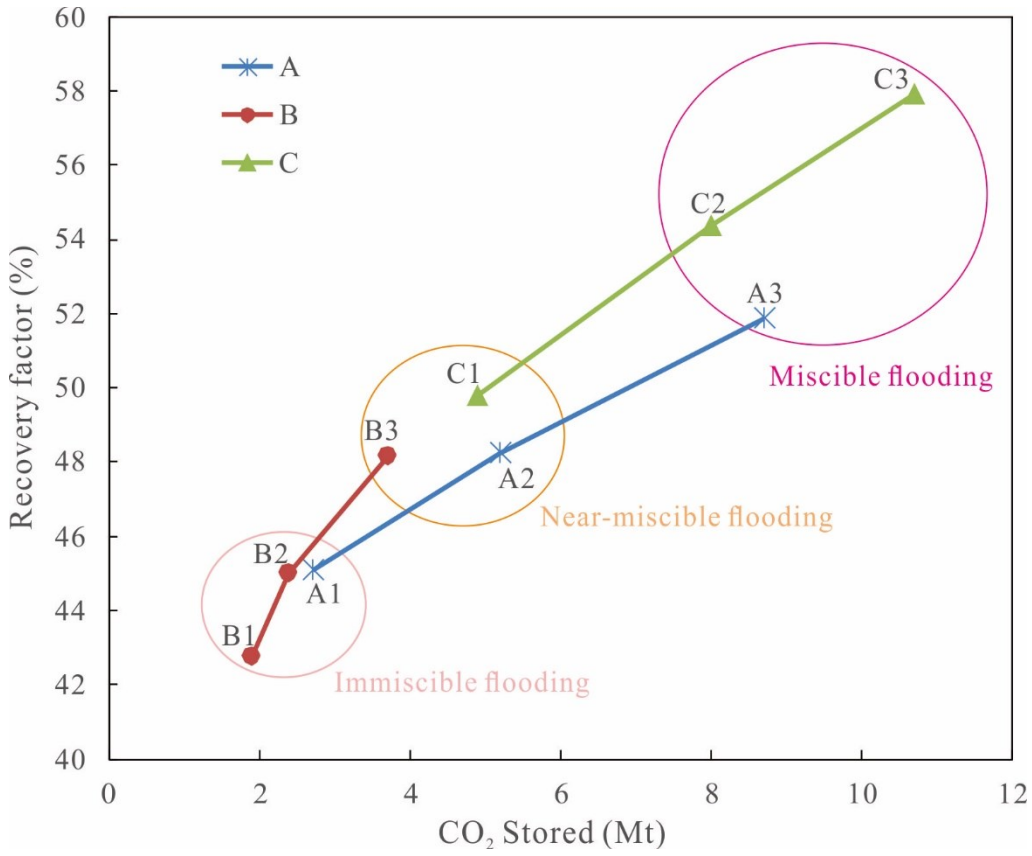

Fig. 16. Correlation curves of the ultimate oil recovery factor and CO_2 stored in the CO_2 flooding scenarios.

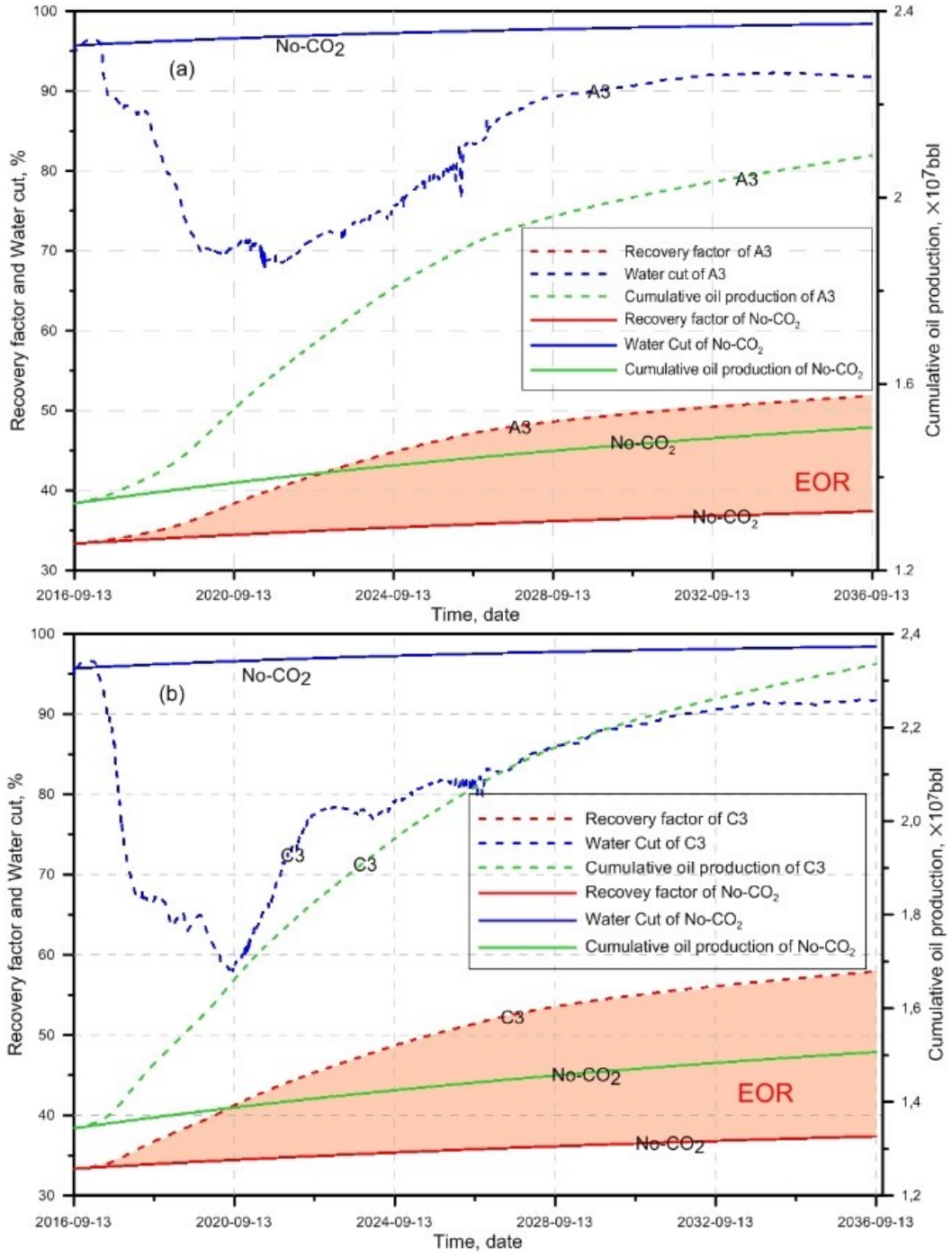

Fig. 17. Result curves of two miscible scenarios, A3 (a) and C3 (b), showing comparisons with the No-CO_2 case for water cut, oil recovery factor and cumulative oil production. The peach shading indicates the enhanced oil recovery factor over the natural depletion (No-CO_2) scenario.

Table 1 Parameters for reservoir characteristics of the HZ21-1 oil field (Liu, 2011)

Reservoir name	Top depth (m)	Closure height (m)	Closure area (km^2)	Reservoir thickness (m)	Porosity (%)	Permeability (mD)	Initial formation pressure (MPa)	Initial formation temperature (°C)	Oil column height (m)	Initial oil saturation (S_{io}, %)	Reserve ($\times 10^4$ m^3)
L30	2,820.7	19.3	7.2	2.6-8.2	15.9	271.3	28.57	125	19.3	61.0	164
$L40_{Up}$	2,842.0	23.0	7.5	9.5-14.5	16.6	317.3	29.01	128	21.7	63.4	368
$L40_{Low}$	2,858.5	23.0	8.9	1.9-5.0	16.2	282.3	-	-	23.0	61.1	134
L45	2,880.0	20.0	7.2	2.8-4.9	12.8	-	-	-	17.1	56.6	33
L50	2,888.2	21.8	7.5	4.0-13.8	14.9	192.3	29.21	131	16.8	61.6	193
L60	2,908.5	22.5	9.2	16.6-27.2	13.5	68	29.64	-	22.5	55.3	387
M10	2,938.5	22.5	9.7	31.0-43.4	15.3	205.3	29.83	132	22.5	59.3	637
M12	3,000.5	11.5	6.6	23.5-30.3	13.7	130.4	-	-	9.0	48.4	39

Note: - represents no test data.

Table 2 Reservoir properties of 6 oil reservoirs in HZ21-1 oilfield for the quick screening

Reservoir properties		L30	L40Up	L40Low	L50	L60	M10
Rock and fluid properties							
Reservoir thickness	H (ft)	19.4	42.7	12.5	27.2	69.9	131.9
Reservoir dip angle	α (^{o})	3.5	3.5	3.5	3.5	3.5	3.5
Permeability in x direction	k_x (mD)	271.3	317.3	282.3	192.3	68	205.3
Oil density	ρ_{oil} (kg/m^3)	798	800	800	802	802	804
CO_2 density	ρ_{CO2} (kg/m^3)*	525	524	534	528	533	534
Oil viscosity	μ_{oil} (cP)	0.32	0.41	0.41	0.36	0.35	0.32
CO_2 viscosity	μ_{CO2} (cP)*	0.054	0.059	0.064	0.066	0.068	0.070
Relative permeability of oil	k_{ro}^o	0.6	0.6	0.6	0.6	0.6	0.6
Relative permeability of gas	k_{rg}^o	0.3	0.3	0.3	0.3	0.3	0.3
Initial oil saturation	S_{oi} (%)	22.7	27.3	25.2	21.2	26.6	25.2
Minimum miscible pressure	MMP (psi)**	3192	3341	3364	3199	3211	3356
Engineering properties							
Well space	L (ft)	900	900	900	900	900	900
Injection pressure	Pinj (psi)	4662	4733	4805	4766	4836	4867
Production pressure	Pp (psi)	2072	2104	2136	2118	2149	2163

* calculated based on formula in Wood (2006); ** estimated based on method from Mungan (1992); other parameters from Liu (2011) and Li et al. (2018).

Table 3 Simulated oil components in the M10 model

Components	CO_2	C_1	C_2	C_3	C_4	C_5	C_{6-12}	C_{13}^+
Composition, %	3.09065	47.4423	6.9656	2.6121	2.6121	1.7414	20.3062	15.2297
Molar mass, g/mol	44.01	16.04	30.07	44.10	58.121	72.15	107.00	237.00

Table 4 Formulas of the dimensionless parameters in the quick screening model (Wood, 2006)

	Symbols	Implications & Calculations	
Input	R_L	Effective aspect ratio	$R_L = \frac{L}{H}\sqrt{\frac{k_z}{k_x}}$
	M_g^o	Mobility ratios between CO_2 and oil	$M_g^o = \frac{k_{rg}^o \mu_o}{k_{ro}^o \mu_g}$
	N_g^o	Buoyancy number	$N_g^o = \frac{H\Delta\rho g\cos\alpha}{\Delta P}$
	P_{injD}	Injection pressure group	$P_{injD} = P_{inj} / P_{MM}$
	P_{pD}	Production pressure group	$P_{pD} = P_p / P_{MM}$
	S_{oi}	Initial oil saturation at the beginning of CO_2 flood	S_{oi}
	S_{orw}	Residual oil saturation to water	S_{orw}
Output	$t_D{}^0$	Dimensionless oil breakthrough time (PV); $t_D^o = 0.346 + 0.102\overline{P_{inJD}} - 0.301\overline{S_{oi}} - 0.118(\overline{S_{orw}} - 0.135)^2 - 0.142(\overline{P_{inJD}} - 0.433)(\overline{S_{oi}} + 0.098) + 0.090(\overline{P_{pD}} + 0.075)(\overline{S_{oi}} + 0.098)$	
	R_{D1}	Dimensionless oil recovery factor at 0.8PV CO_2 injection; $R_{D1} = 38.4 - 7.21\overline{R_L} - 7.15\overline{M_g^o} - 12.4\overline{N_g^o} + 11.4\overline{P_{pD}} + 26.4\overline{S_{oi}} - 7.53(\overline{S_{orw}} + 0.098)^2$	
	R_{D2}	Dimensionless oil recovery factor at 1.0PV CO_2 injection; $R_{D2} = 46.7 - 9.61\overline{R_L} - 7.54\overline{M_g^o} - 11.8\overline{N_g^o} + 6.77\overline{P_{inJD}} + 7.86\overline{P_{pD}} + 27.1\overline{S_{oi}} - 11.7(\overline{S_{orw}} + 0.098)^2$	
	R_{D3}	Dimensionless oil recovery factor at 1.2PV CO_2 injection; $R_{D3} = 48.9 - 9.84\overline{R_L} - 6.45\overline{M_g^o} - 10.2\overline{N_g^o} + 10.2\overline{P_{inJD}} + 6.66\overline{P_{pD}} + 26.4\overline{S_{oi}} - 11.6(\overline{S_{orw}} + 0.098)^2$	
	S_{CO2}	Dimensionless CO_2 storage (PV); $S_{CO2} = 0.571 + 0.161\overline{P_{inJD}} - 0.080\overline{P_{pD}} + 0.050(\overline{P_{inJD}} - 0.135)^2 + 0.033(\overline{P_{inJD}} + 0.075)^2 - 0.113(\overline{P_{inJD}} - 0.433)(\overline{P_{pD}} + 0.075)$	

Note: the output parameters with a horizontal line above are the values normalized to between -1 and +1.

Table 5 The CO_2 flooding scenarios designed in simulation

Injection well / Injection pressure	I1	I2	I1+I2
5000 psi	A1	B1	C1
5500 psi	A2	B2	C2
6000 psi	A3	B3	C3

Table 6 The dimensionless outputs from the quick screening model of the HZ21-1 field

Reservoirs		L30	L40Up	L40Low	L50	L60	M10
Dimensionless outputs							
Breakthrough time	$t_D{}^o$ *(PV)*	0.70	0.61	0.65	0.74	0.64	0.66
Oil recovery at 0.8*PV*	R_{D1}*(%)*	12.82	30.06	4.20	17.26	36.13	33.95
Oil recovery at 1.0*PV*	R_{D2}*(%)*	21.07	42.95	8.89	27.41	51.27	48.94
Oil recovery at 1.2*PV*	R_{D3}*(%)*	24.09	45.99	11.28	30.85	54.89	52.49
CO_2 storage	S_{CO2} *(PV)*	0.80	0.78	0.79	0.81	0.81	0.80
Reserve percentage	*Q(%)*	8.35	18.73	9.72	12.47	19.69	32.42

Note: *Q* is the percentage of each reservoir's reserve to the total of the six reservoirs.

Table 7 Simulation results of CO_2 injection and No-CO_2 scenarios

Scenarios	Reservoir pressure during CO_2 flooding /psi		CO_2 flooding mechanism	CO_2 injection rate /$\times 10^4$ t/a			Cumulative CO_2 injection /$\times 10^6$ t	Cumulative CO_2 production /$\times 10^6$ t	Total CO_2 stored /$\times 10^6$ t	Cumulative oil production ($\times 10^7$bbl)	Ultimate total recovery factor /%	CO_2 flood enhanced recovery factor /%	CO_2 to oil exchange ratio (t CO_2/t_{oil})
	Max.	Mean		Max.	Min.	Ave.							
A1	4,361	4,229	Immiscible	14.3	1.8	12.0	12.4	9.8	2.7	1.8	45.08	7.71	4.2
A2	4,627	4,395	Near-miscible	24.9	2.8	20.1	21.1	15.9	5.2	1.9	48.24	10.87	6.2
A3	5,295	4,794	Miscible	53.2	3.7	37.9	39.5	30.8	8.7	2.1	51.85	14.48	8.4
B1	4,320	4,182	Immiscible	12.1	2.4	10.5	10.7	8.9	1.9	1.7	42.73	5.36	3.6
B2	4,502	4,208	Immiscible	18.6	3.7	16.7	17.0	14.6	2.4	1.8	44.98	7.61	3.8
B3	4,839	4,325	Near-miscible	32.7	5.1	29.7	30.1	26.3	3.7	1.9	48.14	10.77	4.6
C1	4,517	4,331	Near-miscible	25.8	4.8	19.9	20.4	15.6	4.9	2.0	49.80	12.43	5.3
C2	4,813	4,498	Miscible	45.0	7.6	35.6	36.5	28.5	8.0	2.2	54.36	16.99	6.8
C3	5,269	4,877	Miscible	79.2	10.5	57.8	59.0	48.3	10.7	2.3	57.92	20.55	7.8
No-CO_2	3,996	3,957	-	-	-	-	-	-	-	-	37.37	-	-

Note: Reservoir pressure, injection rate, cumulative CO_2 injection and production, cumulative oil production are derived from outputs of the GEM simulations.